Marine Geology 380 (2016) 245–263

Contents lists available at ScienceDirect

Marine Geology

journal homepage: www.elsevier.com/locate/margo

Investigation of deep sea shelf sandbank dynamics driven by highly energetic tidal flows

Antonia Chatzirodou *, Harshinie Karunarathna, Dominic E. Reeve

Energy and Environment research Group, Zienkiewicz Centre for Computational Engineering, College of Engineering, Swansea University, Singleton Park, Swansea SA2 8PP, UK

ARTICLE INFO

Article history:
Received 24 April 2015
Received in revised form 19 March 2016
Accepted 20 April 2016
Available online 22 April 2016

Keywords:
Pentland Firth
Tidal energy extraction
Sandbanks
Delft3D model
Sediment transport modelling
Morphodynamics

ABSTRACT

In this paper we describe a numerical modelling study carried out to investigate the prevailing sediment dynamics of two large sandbanks located at a site designated for future development of tidal stream energy extraction, in the Inner Sound Channel of Pentland Firth, Scotland, UK. A calibrated and validated 3D Delft3D hydrodynamic model covering Pentland Firth channel was combined with a morphodynamic model. The sea bed changes occurring around the sandbanks during a period of two spring-neap tidal cycles are described and discussed in detail. It was found that both sandbanks, which are located in a deep shelf region (depths > 18 m), are morphodynamically active and their existence and integrity are strongly linked with the existing hydrodynamic regime.

1. Introduction

The tidal energy sector is a rapidly growing industry both in the UK and beyond (EOEA, 2012). The commercial interests are now moving towards deployment of large arrays of tidal energy extraction devices. In relation to the installation of large scale tidal turbine arrays numerous factors, many quite uncertain at the moment and linked to site specifications, will determine the array location and operating characteristics. One such factor that will play an important role in any decision making process is the associated impact of in-stream tidal energy converters on the ambient marine environment (Schlezinger et al., 2013; Fallon et al., 2014; Waggitt and Scott, 2014).

A particular concern is the extent to which changes to the tidal currents arising from energy extraction will impact the natural sediment transport regime and hence the sea bed morphology. Due to the sparseness of sediment data in most deployment sites, only very limited studies have so far included the impacts of tidal energy extraction on sediment transport and morphology (Neill et al., 2009; Neill et al., 2012; Robins et al., 2014). In-stream tidal turbines will decrease the flow velocities in the vicinity of the array layout, as well as notable reductions in current flows will occur even beyond the boundaries of the array (Neill et al., 2012). As bed shear stresses have a quadratic dependence on flow velocity, sediment transport has an even higher power of dependence on flow velocity (Soulsby, 1997). As a result, tidal energy extraction may have a much greater influence on the tidally induced sediment transport patterns than on the tidal currents. As part of the environmental impact assessment of new large scale tidal turbine array installations, it is essential that the existing sediment dynamics responsible for the maintenance mechanisms of the observed sea bed sedimentary structures in and around turbine array deployment sites are investigated and understood.

The selected site for this study is Pentland Firth, which divides the Scottish mainland from the Orkney Islands (Fig. 1). It is considered to be one of the most favourable sites for tidal energy harvesting in the UK, due to the prevailing extremely high tidal flows (Couch and Bryden, 2008). The main aim of this research is to understand the sediment transport and morphodynamic environment of the existing seabed in the Inner Sound Channel in Pentland Firth, where large scale tidal current turbine array installations may take place in future. We used a rigorously tested and widely used Delft3D coastal area model to investigate the response of sea bed sediment dynamics to 3D flow structure of the Inner Sound Channel. The existence, integrity and evolution of two large sandbanks in the Inner Sound Channel, which have significant morphological and ecological value, will be examined in detail by linking their morphodynamics with the existing flow regime. The type of sandbanks studied in this research is typical of the sand deposits that may form and exist closer to tips of islands and in areas where complex tidal current regimes force sediment to accumulate into finite spaces while the surrounding areas are largely sediment free (Bastos et al., 2003; Berthot and Pattiaratchi, 2006). As a result, even though the results presented in this study are site specific, the generic methodology employed in the investigation should have wider application.

* Corresponding author.
E-mail address: 684449@swansea.ac.uk (A. Chatzirodou).

http://dx.doi.org/10.1016/j.margeo.2016.04.011

Fig. 1. "The Pentland Firth site." 58°42′58.97″ N and 3°06′53.47″ E. Google Earth. January 1, 2004. December 16, 2015; Upper left figure: "United Kingdom." 55°30′41.31″ and 3°21′25.69″. Google Earth. April 10, 2013. December 16, 2015.

In Section 2, an overview of the complex tidal flows inside the Inner Sound channel is given. In Section 3, the sediment coverage and characteristics inside Pentland Firth, Inner Sound channel are described. Section 4 explains the methodology used. In Sections 5 and 6 the morphodynamic environment of the two large sandbanks located in this area is modelled and discussed. Section 7 concludes the paper.

2. Overview of the hydrodynamics of Inner Sound Channel

Pentland Firth (PF), located between Orkney Islands and the north of Scottish mainland joins the Atlantic Ocean and the North Sea (Fig. 1). Differences in tidal range and phase at both ends of the PF result in tidal currents of up to 8 m/s in certain locations for 2.5 m head drop over a tidal cycle. This provides an abundant energy resource for tidal current turbine deployments (Baston and Harris, 2011). The Inner Sound channel separates the Island of Stroma in Pentland Firth and the Scottish Mainland (Fig. 1). Water depths between 25 and 30 m coupled with fast moving tidal flows in the Inner Sound Channel provide a very favourable collation of site characteristics for tidal energy extraction (Easton et al., 2010; Goddijn-Murphy et al., 2013). The complex 3D hydrodynamic environment of this area has been extensively investigated in previous work through numerical modelling studies (Baston and Harris, 2011; Baston et al., 2013; Chatzirodou and Karunarathna, 2014).

Chatzirodou and Karunarathna (2014) used a large scale 3D hydrodynamic model Delft3D (Lesser et al., 2004) to reproduce the dynamics of tidal flows in Pentland Firth. A shelf wide flow model developed by Baston et al. (2013) was used to obtain boundary conditions for this large scale model. The model was able to capture the existing hydrodynamics of Pentland Firth during a period of two spring-neap tidal cycles (09/09/2001–09/10/2001). Results from this large scale hydrodynamic model produced appropriate boundary conditions for a nested higher resolution hydrodynamic and morphodynamic model covering the Inner Sound channel (Fig. 2), which will be used in this study.

The detailed hydrodynamic study of the Inner Sound Channel revealed that at spring ebb phase, a channel flow was formed and travelled further offshore from the western side of the Island of Stroma. Strong ebb currents exited the North-West part of Inner Sound with 200°–250° flow direction. At spring flood phase, a tidal jet was formed to the south of the ebb channel flow and travelled eastwards in a constrained path located in the middle part of Inner Sound channel. Maximum flood flows were observed inside the central part of the tidal jet whereas decreasing velocity gradients were observed further eastward (Chatzirodou and Karunarathna, 2014). Overall, a distinct

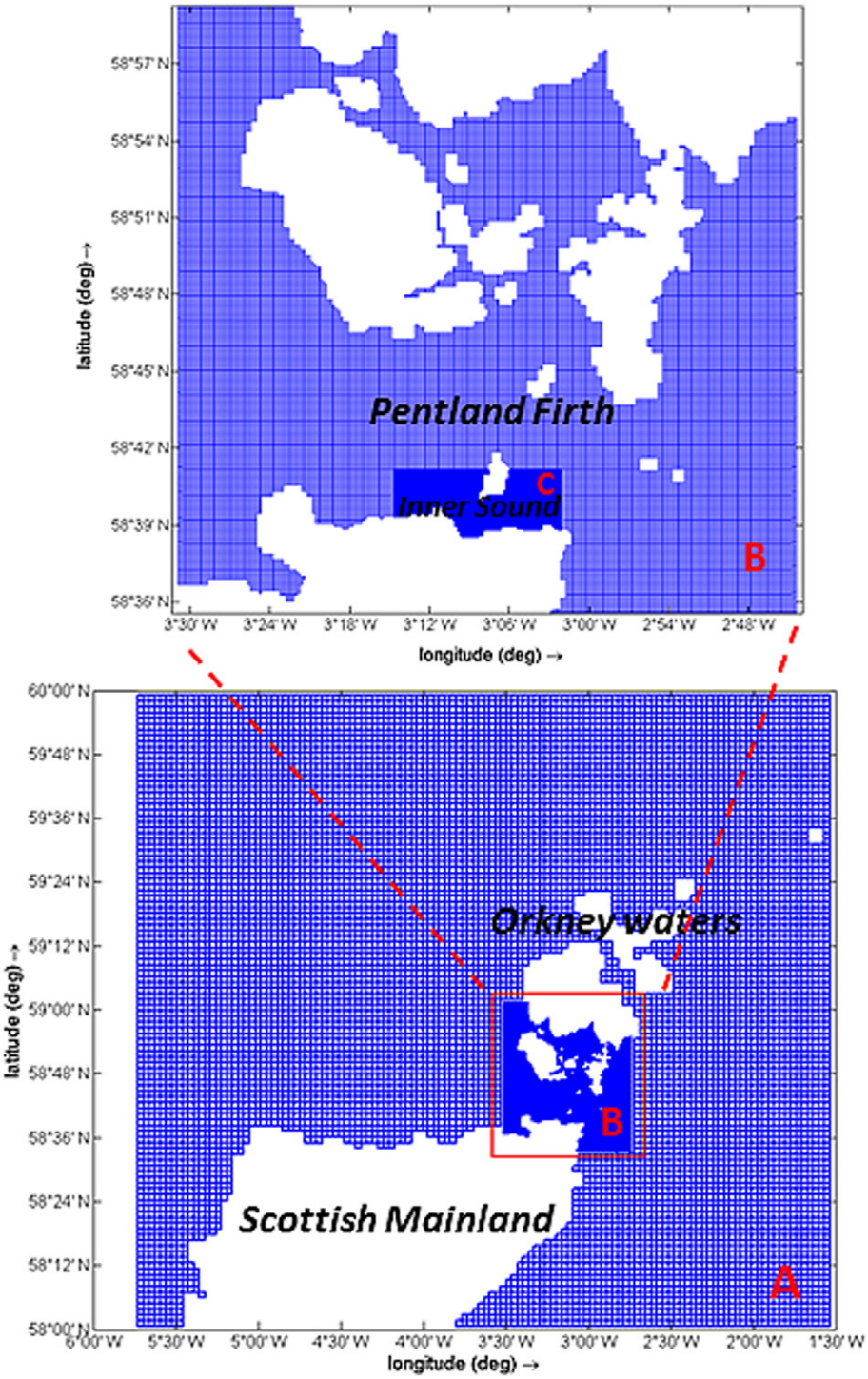

Fig. 2. Large scale hydrodynamic model domain used to investigate 3D flow dynamics of Pentland Firth and the small high resolution Inner Sound channel model used in this study. A: Shelf wide model (2 km * 2 km), B: Large scale model of Pentland Firth (200 m * 200 m) and C: Small scale high resolution model of the Inner Sound Channel (60 m * 60 m).

inequality occurred in response to the strength and directionality of the computed channel flows between the ebb and flood phase. The asymmetry found between maximum ebb and flood currents in Inner Sound channel revealed a notable residual circulation pattern at both sides of the Island of Stroma, and close to the areas where the two large sandbanks, investigated in this study, are observed. Residual flow patterns are found to be notably weaker than the transient flow characteristics. As a result, bed shear stresses on the sandbank areas exceed their critical value during maximum ebb and flood flows, which may lead to sediment movement.

3. Sand coverage inside Pentland Firth, Inner Sound Channel

British Geological Survey (BGS) (2013) particle size data around the UK and a series of benthic video trawls conducted by Marine Scotland Science (MSS) in 2010 in Scottish waters were used to describe sand coverage, sediment characteristics and sea bed morphology in the Pentland Firth, Inner Sound channel. Data were provided by the EPSRC funded Terawatt project (EP/J010170/1). Both BGS (2013) and MSS (2010) data were post-processed in Delft3D-Quickin suite (Deltares, 2011) to develop a sediment coverage map in the Pentland Firth

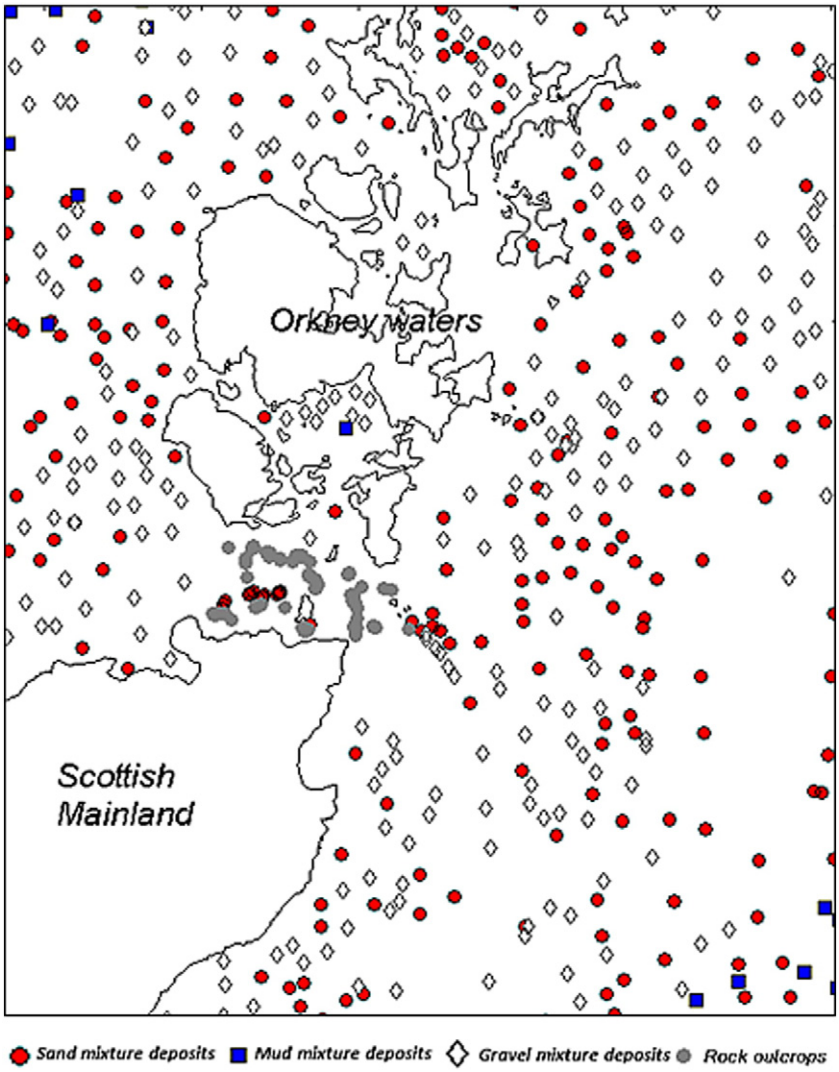

Fig. 3. Description of sand coverage in Pentland Firth channel by use of both BGS particle size data (2013) and MSS database of benthic video trawls (2010). Data were processed in Delft3D-Quickin suite (Deltares, 2011).

(Fig. 3). It can be seen in Fig. 3 that sediment availability in this area is limited and that most of the seabed consists of sediment free bedrock. However vast shell sand deposits lying on scoured bedrock are abundant in some areas (Shields et al., 2009). The recorded sediment data inside Pentland Firth reveal a highly spatially variable natural sediment dynamics environment. Despite the scarcity of data, MSS (2010) images of the seabed in Pentland Firth channel reveal regions of a broad range of seabed types presented in Fig. 4, which includes sand veneers on scoured bedrock, large cobbles with ponded sand and gravel zones, large regions of sand waves and sandbank areas.

A few available MSS (2010) sediment samples also reveal some sand deposits eastward in the lee side of Stroma, which was confirmed by Easton et al. (2011). A rippled sandy region lying directly in the lee of the Island of Stroma and a sandbank area north-eastward of the Inner Sound, were found to be of significant extent. It was found that the location of the sandbank area north-eastward inside Inner Sound coincides with a convergent zone between peak ebb and flood currents. Regions of sediment accretion have been also formed in the observed sandy region, in the leeward side of Stroma (Easton et al., 2011).

A wide range of sea bed types inside the Inner Sound channel has been identified by MeyGen (2012), based on a Klein 3000 side-scan sonar geophysical survey conducted by iXSurvey (2009). This report reveals the presence of scoured bed rock areas, gravel and cobble dominated seafloor lying upon rock outcrops and coarse sand-grained sandbank regions, unevenly distributed around the southward tip of the Island of Stroma.

iXSurvey (2009) revealed a large pear shaped sandbank (A) located north-eastward inside the Inner Sound channel. This sandbank lies in a SW–NE direction, making approximately 60° with the North and with a maximum height of ~15 m above the surrounding maximum water depth of ~35 m on scoured bedrock. The depth gently decreases towards the crest of the bank in the north-eastern side. The sandbank is almost 3 km long and 1 km wide and is characterized by discrete large and medium size sand waves with maximum length (L) of 20 m and height (H) of 0.5 m. A smaller scale sandbank region (B) located in the westward side of the Island of Stroma in NW–SE direction at a maximum depth of approximately 33 m has also been discovered. Large sand ripples of approximately 14 m length and 0.2 m height were found to cover the whole bank area. As already identified by Easton et al. (2011), a less expanded sandbank (C) where small sand ripples are formed, was observed directly in the lee of the Stroma southward of Mell Head. This sea bed feature is oriented NE–SW, parallel to the coastline. The remaining seabed areas of the Inner Sound channel consist of sediment free, non-erodible bed rock.

MeyGen (2012) also presents analyses of the sediment grain size distribution within the most significant seabed features identified above, based on sediment sampling surveys conducted by the Aquatic Survey and Monitoring Ltd. (ASML). The sea bed samples consist of

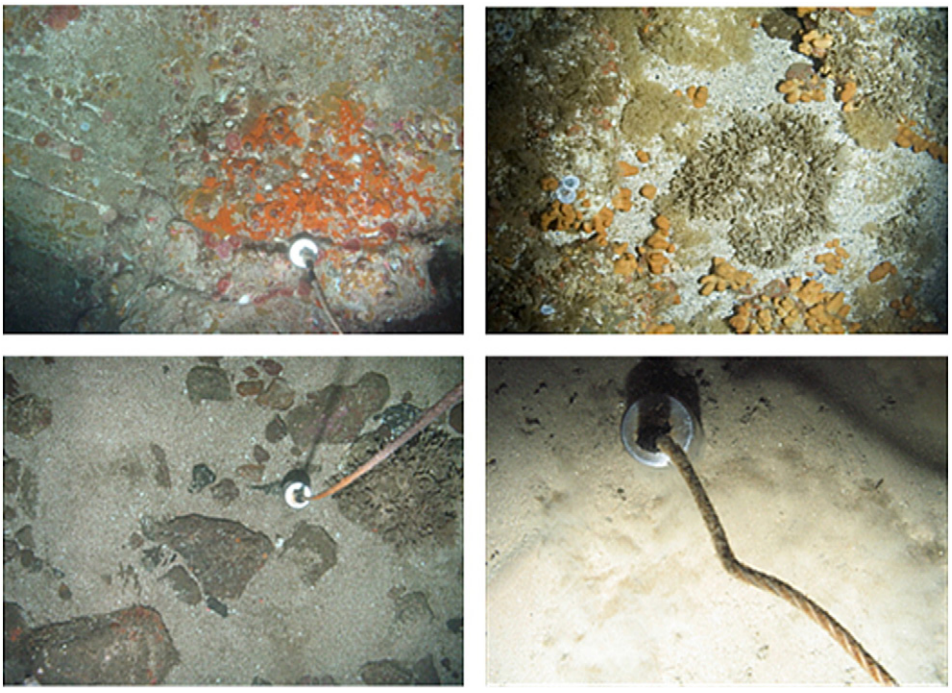

Fig. 4. Images from MSS database of benthic video trawls (2010) showing various seabed structures found in Pentland Firth channel.

>50% of coarse sand and fine gravel (1–4 mm) on the sandbank (A), lying at water depths in between 18 and 30 m. In contrast, the small-scale westward sandbank (B) located in deeper areas (~30–35 m) is mostly covered by coarser sand and fine gravel with grain sizes between 2 mm and 5 mm. On the bed form (C), finer sand was found at the north side in contrast to coarser sand found at the outer side southward. Bedrock outcrops and discontinuous thin veneer of sandy gravel and cobbles, free from discrete transversal bed forms, were also recognized in the intermediate areas.

Based on MeyGen (2012) observations, which were verified by BGS (2013) and MSS (2010) data and literature findings of Easton et al. (2011), a sea bed feature map including the sandbanks A, B and C was reconstructed inside Inner Sound, using the Delft3D-Quickin suite (Deltares, 2011). The sandbanks are located in very close proximity to the proposed large scale tidal turbine array in the Inner Sound Channel (Fig. 5) (Meygen, 2012). The sandbank C is of much smaller size compared to the sandbanks A and B. Therefore, this study will focus on the dynamics of the two largest sandbanks, which may be most likely influenced by the change in tidal current regime due to tidal energy extraction in future.

4. Morphological model set up

To investigate the morphodynamic environment of two sandbanks (A, B), open source Delft3D, D-Morphology modelling suite, developed by Delft Hydraulics (Lesser et al., 2004) is used. The programme utilizes a finite difference representation of the unsteady swallow water equations in 3 dimensions to compute sediment transport processes (both suspended and bed load rates) and morphological changes. In the vertical direction momentum equation reduces to a hydrostatic

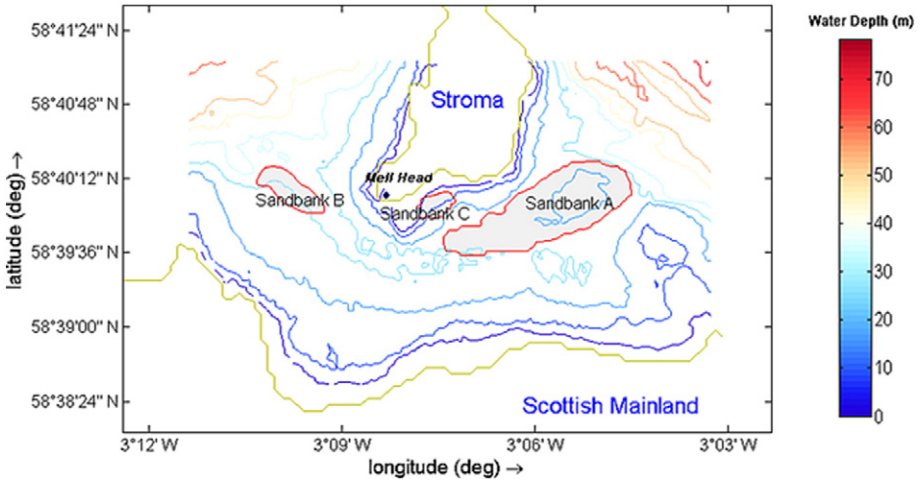

Fig. 5. Sea bed features map inside Inner Sound channel has been reconstructed using Delft3D Quickin suite (Deltares, 2011). Sandbank availability data were taken from observations found in MeyGen (2012) and having been verified by BGS (2013) and MSS (2010) data and literature findings (Easton et al., 2011). Grey patches denote mobile sandbank areas A, B, C. The intermediate regions are covered by non-erodible rock substratum. The colour bar indicates water depth values (m).

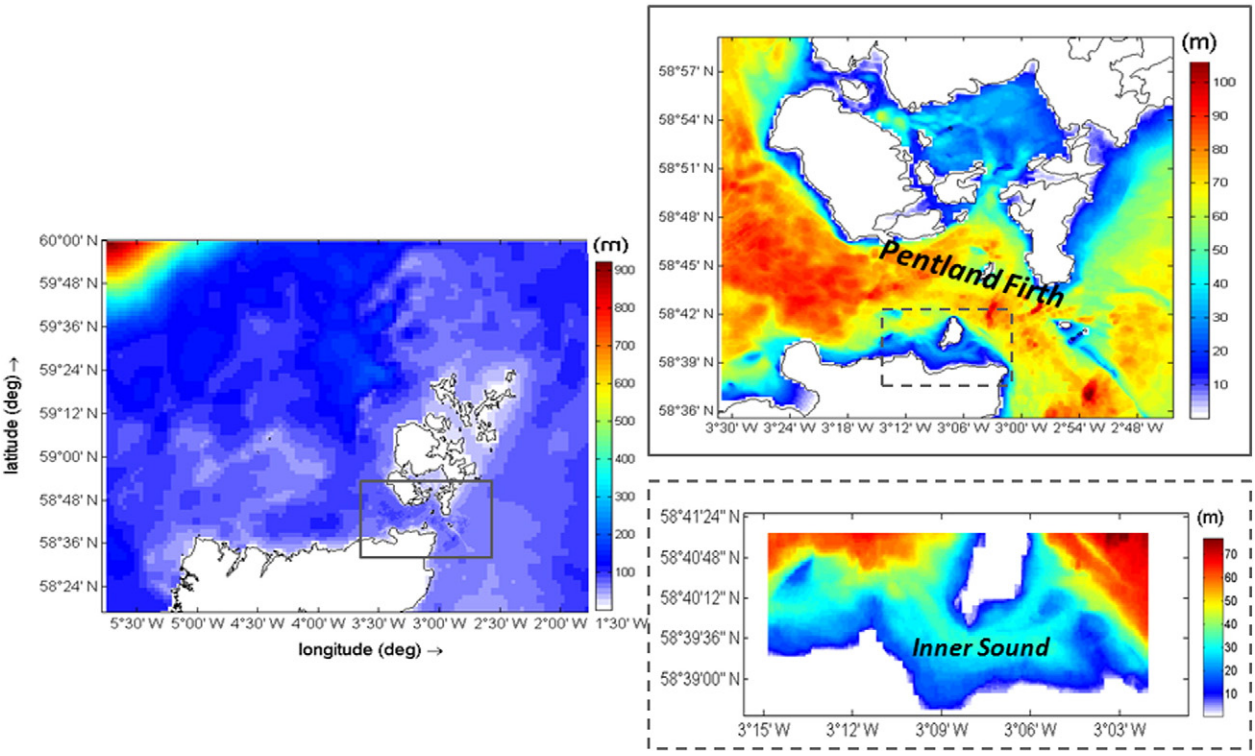

Fig. 6. The hydrodynamic mesh is mapped onto gridded bathymetry data available at (20 m * 20 m) resolution. The colour bars indicate water depth values (m).

pressure assumption since accelerations due to buoyancy terms and abrupt variations in complex topographic features are assumed to be small, in comparison to gravitational acceleration (Lesser et al., 2004). A staggered grid with varying resolution from 200 to 2000 m in deeper areas in Pentland Firth and 66 m in Inner Sound was set up. The model domain extends from 58°00′N to 60°00′N and from 5°44′W to 1°32′W (Fig. 2). The tidal forcing conditions along the open boundaries of the domain were generated by the TPXO 7.2 Global Inverse Model (Egbert et al., 1994), based on the major semi-diurnal (M2, S2, N2, K2) and diurnal (K1, O1, P1, Q1) tidal constituents. Model bathymetry data were taken from The Crown Estate (TCE), UK, the organization responsible for authorizing the leasing of sea bed areas in the UK waters for tidal and wave energy extraction. The gridded bathymetry data available at 20 m resolution were mapped onto the model domain, thus allowing for a detailed representation of a very complex bathymetry (Fig. 6).

In the vertical water column, the computational grid is defined by σ-coordinates (Lesser et al., 2004). A 3D model will resolve with higher accuracy, in comparison to a 2D model, the complex tidal flows and consequently the bed evolution patterns (Jones et al., 2006). To increase the efficiency of the 3D model and to maintain the computation time at

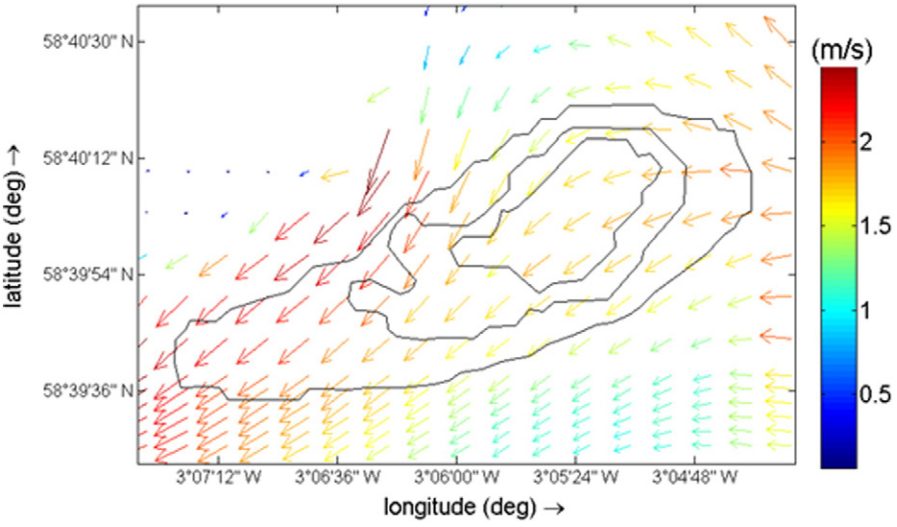

Fig. 7. Horizontal velocity (m/s) at the bottom layer, at maximum spring ebb tide (19/09/2001 2:40) on the sandbank A. Continuous black lines denote the extent of the sandbank. The colour bar indicates the magnitude of velocity and arrows indicate velocity direction.

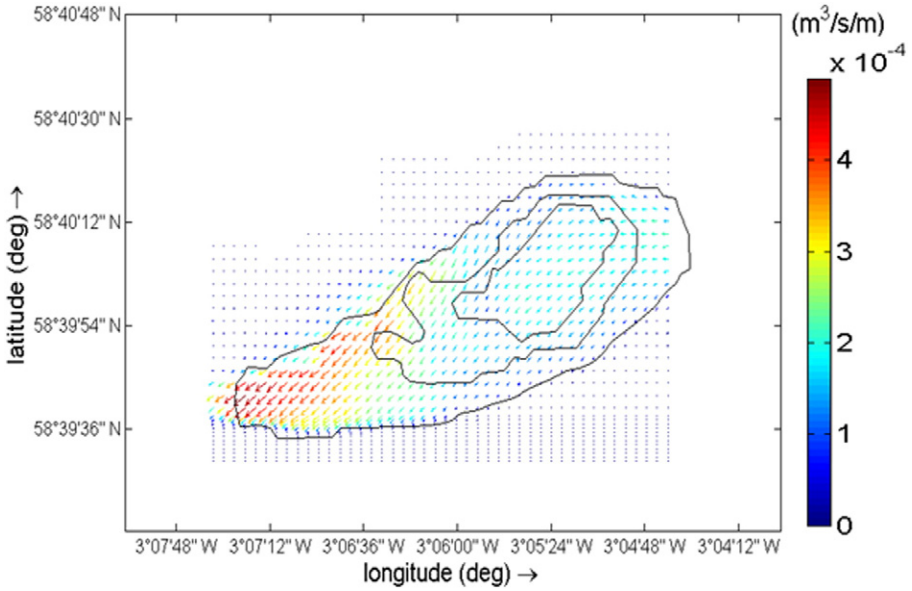

Fig. 8. Bed load sediment transport rates ($m^3/s/m$), at maximum spring ebb tide (19/09/2001 2:40) on the sandbank A. Continuous black lines denote the extent of the sandbank. The colour bar indicates the magnitude of sediment transport rates and arrows indicate sediment transport direction.

acceptable level a compromise needs to be made between the number and the vertical structure of the selected σ-layers. Ten equidistant σ-layers were used in the present study.

In all computations presented in this paper, a constant Chezy value of 50 $m^{1/2}/s$ was used as the representative magnitude of the regional roughness of the sea bed in the modelled area. The validated model, introduced in Section 2, showed that the best agreement between the modelled and measured current velocity profiles was found when a constant bed roughness value of 50 $m^{1/2}/s$ was used. A detailed study on calibration and validation of the models can be found in Chatzirodou and Karunarathna (2014). Higher Chezy values represent a smoother bed whereas lower values represent a rougher bed. It is understood that sediment transport strongly depends on local sea bed roughness which in turn is influenced by migrating bed forms generated by sand movements. However, due to the scarcity of the data, we will not be able to consider spatial variability of the bed roughness.

A key feature of the D-Morphology suite is that it allows the computed flows to adjust to local bed level changes. The model solves the governing equations and dynamically feeds back to the bedload sediment transport formula used in present work in order to determine sediment transport vectors and hence bed change. The water depth at grid cell centres is updated based on the change in quantity of the bottom sediment in each control volume. The bed shear stress used to calculate the bed load transport rates is taken from the downwind cell faces. The bed level at the inflow boundaries, covered by non-erodible regions is prescribed assuming zero sea bed variations.

The turbulent flows are vertically resolved by applying the κ-epsilon turbulence closure model (TCM). The horizontal eddy viscosity term which represents the turbulent length scales generated by the flow in

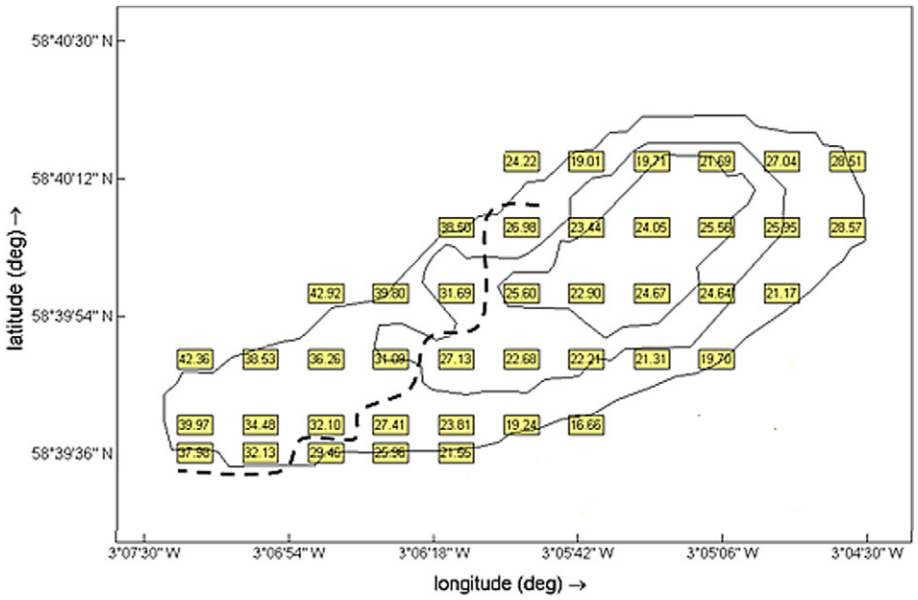

Fig. 9. Bed shear stresses (N/m^2) at maximum spring ebb tide (19/09/2001 2:40) on the sandbank A. Continuous black lines denote the extent of the sandbank. The regions above the black dashed line denote the parts of maximum bed shear stresses which significantly exceed the critical bed shear stress magnitude on the north-western flank of the sandbank.

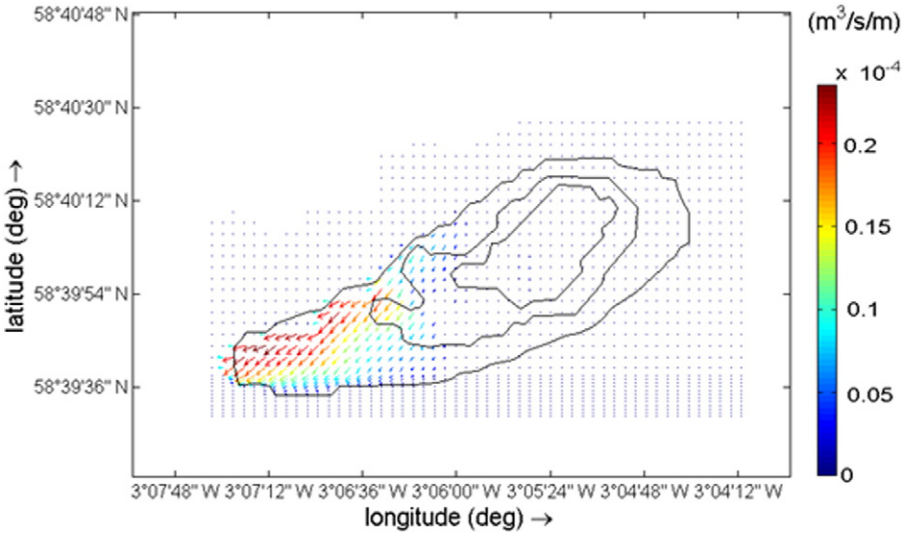

Fig. 10. Bed load sediment transport rates ($m^3/s/m$) close to slack water time (19/10/2001 5:20) on the sandbank A. Continuous black lines denote the extent of the sandbank. The colour bar indicates the magnitude of sediment transport rates and arrows indicate sediment transport direction.

the horizontal direction is partly approached by a constant background value which varies from 10 to 1 m^2/s in the higher resolution grids. In 3D simulations the horizontal eddy viscosity is eventually calculated at each σ-layer, as the sum of the constant background value and the vertical eddy viscosity, computed from the turbulent closure model.

In the present model setup, Van Rijn (1993) sediment transport formula is used to calculate bed load transport rates. For a flat-bed case and for tidally induced near bed load transport, the Van Rijn (1993) formula reads:

$$|S_b| = 0.5\rho_s SedD_{50} u_*' D_*^{-0.3} T \quad (1)$$

where $|S_b|$ (kg/m/s) is the bed load transport rate; u_*' (m/s) is the effective bed shear velocity related to grains; D_* is the dimensionless particle diameter; T represents the dimensionless bed shear stress; ρ_s (kg/m^3) is the density of the sediment fraction and $SedD_{50}$ (m) equals to the median grain size diameter. Both u_*', T are calculated from the velocity assigned to the first computational layer above the seabed. The sediment size is assumed to follow a piece-wise log uniform distribution.

Berthot and Pattiaratchi (2006) found that tidal flows predominantly contribute to preserve existing sandbanks and that the sediment grain size and availability of sand will not play an important role once sandbanks are formed. Thus in the present model set up, a single sediment size ($SedD_{50}$) value of 3 mm (3000 μm) on the north-east crest and 2 mm (2000 μm) on the south-west flank are used for the sandbank A area. A single $SedD_{50}$ value of 4 mm (4000 μm) is selected for the sandbank B. The immobile areas lying in between the sandbanks and further offshore on the rest of locations will represent non-erodible regions for the morphodynamic simulations.

The magnitude and direction of bed load transport rates are computed based on the formulation presented in Eq. (1). The direction of sediment transport is aligned with the tidal flows at the bottom computational layer. Then a first-order upwind numerical scheme is used to transfer bed load transport components from the water level points to U (x

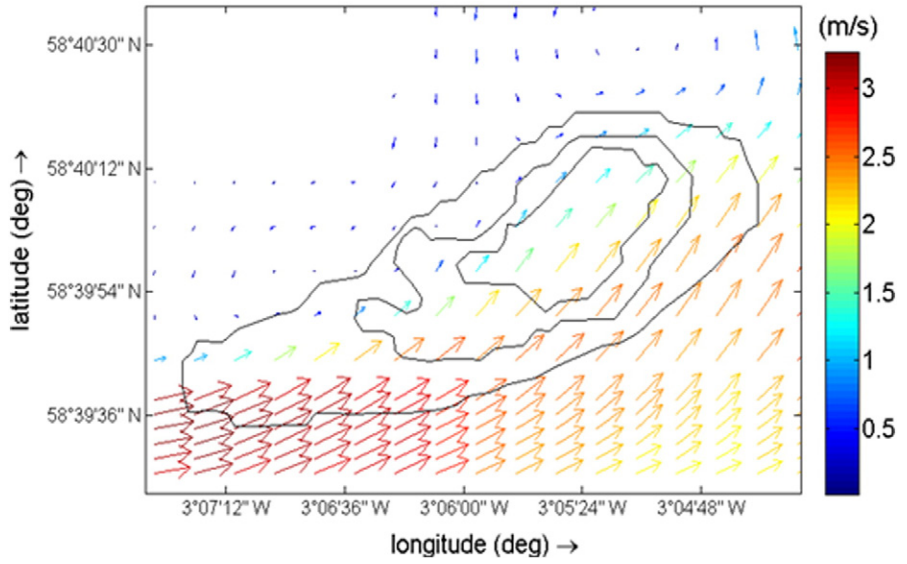

Fig. 11. Horizontal velocity (m/s) at the bottom layer, at maximum spring flood tide (19/09/2001 8:00) on the sandbank A. Continuous black lines denote the extent of the sandbank. The colour bar indicates the magnitude of velocity and arrows indicate velocity direction.

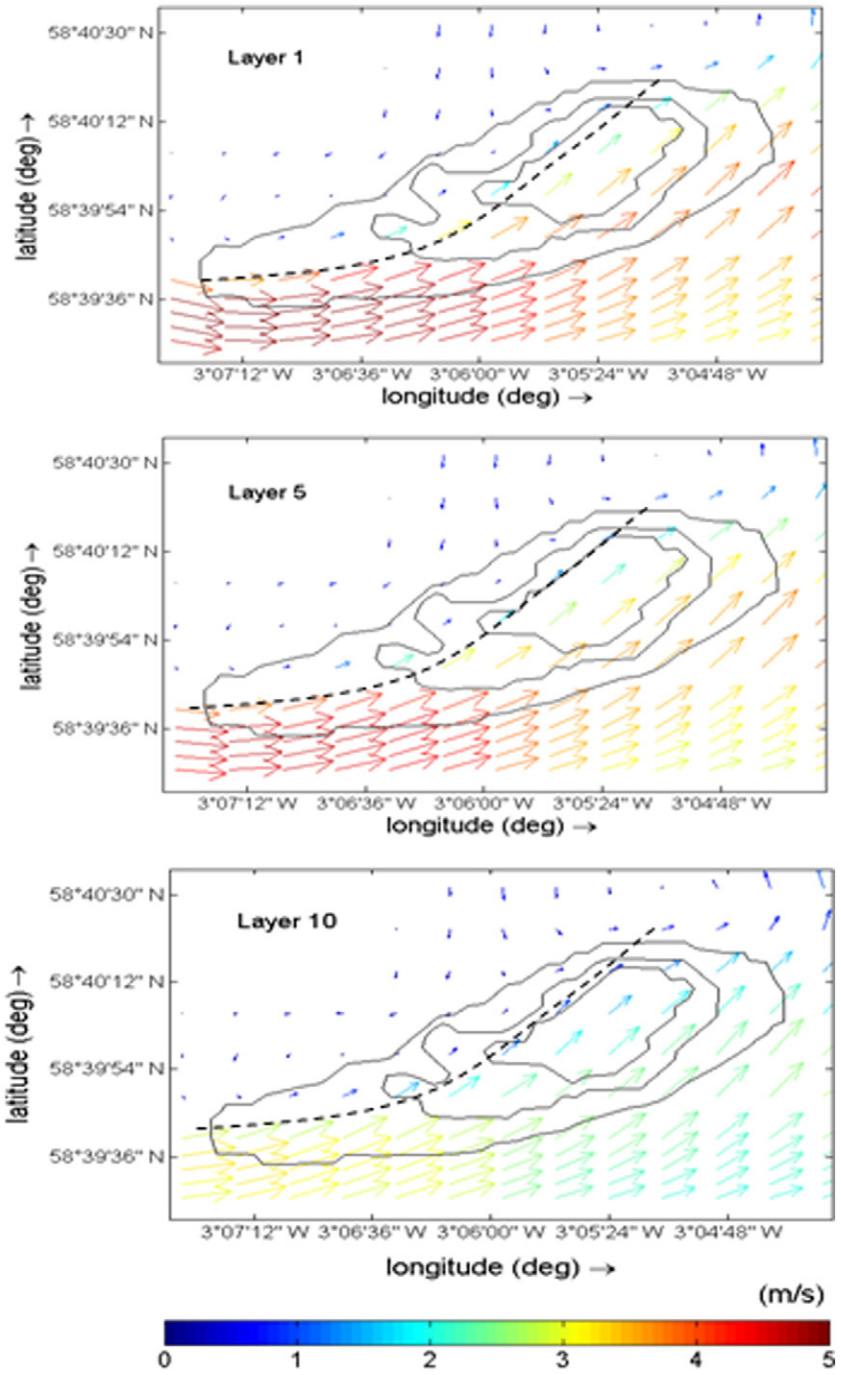

Fig. 12. Horizontal velocity vectors (m/s) at surface (σ-layer 1), middle (σ-layer 5) and bottom layer (σ-layer 10) on the sandbank A, at maximum spring flood tide (19/09/2001 8:00). Continuous black lines denote the extent of the sandbank. The upper most part of the black dashed line denotes the areas where currents veer and form small scale cyclonic eddies throughout the entire water column. The colour bar indicates the magnitude of velocity and arrows indicate velocity direction.

direction) and V (y direction) velocity points and ensure numerical stability. The transport vectors are further corrected for bed-slope effects.

The selection of Van Rijn (1993) bed load transport formula is considered appropriate and may be used to calculate sediment movements of coarser sand particles with $SedD_{50}$ exceeding the value of 2 mm (2000 μm). However, it has been found that a deterministic bed load transport model used for coarse-grained sands will possibly underestimate the predicted sediment transport rates (Nelson et al., 1995; Kleinhans and Van Rijn, 2002; Van Rijn, 2005). The critical bed shear stress magnitude will increase, in response to the classical Shields curve at higher median grain size ($SedD_{50}$) values leading to prediction of lower sediment transport rates. It has also been proved that near-bed turbulent structures may result in notably high transport rates even if the computed bed shear stress is below the critical Shields value (Kleinhans and Van Rijn, 2002) and that a deterministic bed load transport model can be less appropriate for flows above complex bed topography where turbulent boundary layers are developed (Nelson et al., 1995; Lefebvre et al., 2014). Inside the Inner Sound channel the gradually changing bathymetric profile results at least locally in a less complex topography. Following that it can be argued that the

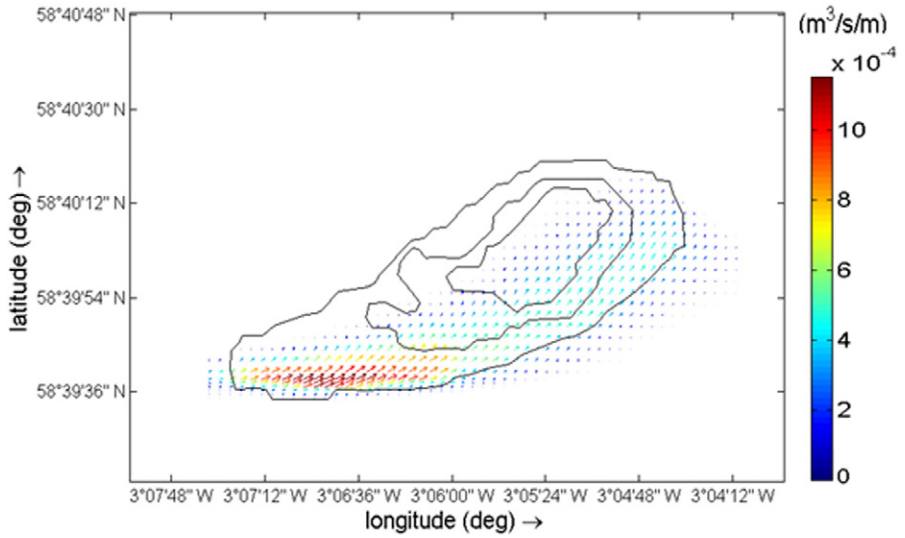

Fig. 13. Bed load sediment transport rates ($m^3/s/m$), at maximum spring flood tide (19/09/2001 08:00) on the sandbank A. Continuous black lines denote the extent of the sandbank. The colour bar indicates the magnitude of sediment transport rates and arrows indicate sediment transport direction.

deterministic Van Rijn (1993) bed load transport formula allows calculation of sediment movements with sufficient accuracy.

It should be noted that considering the type of sediment present on the sea bed and the unavailability of any measurements, suspended sediment transport was excluded in this study. This assumption is supported by the work of Bastos et al. (2004) and Berthot and Pattiaratchi (2006) who argued that bed load transport alone is the governing mode of sediment transport in shelf bank areas where sediments range from medium to mobile coarse sand.

In case of a cold start to model runs where the hydrodynamic model takes time to stabilize the erosion/accretion patterns will not reflect realistic morphological changes and should be ignored. It is found, through experimental model runs that initial conditions need approximately 23 h to adapt to boundary conditions. Therefore, a spin up time of 1440 min was set before morphological updating starts. If the quantity of bottom sediment is limited and less than a user-defined threshold value the calculated bed load transport is scaled down to prevent significant erosion and to assure the availability of sediment for the transport calculations. The non-erodible areas will accumulate a small amount of sediment so as to allow for an equilibrium transport pattern to evolve.

5. Morphodynamics of the sandbank A

The existing sediment transport patterns and morphodynamics of the sandbank areas A and B in the Inner Sound channel, which are located at very close proximity to a proposed large scale tidal turbine array installation, are of particular interest here. In many places, sub tidal banks which lie few kilometres away from the coastline, can be of significant importance to the coastal environment (Dyer and Huntley, 1999). Their presence can serve as an important feeding ground for fish populations and is associated with the existence of

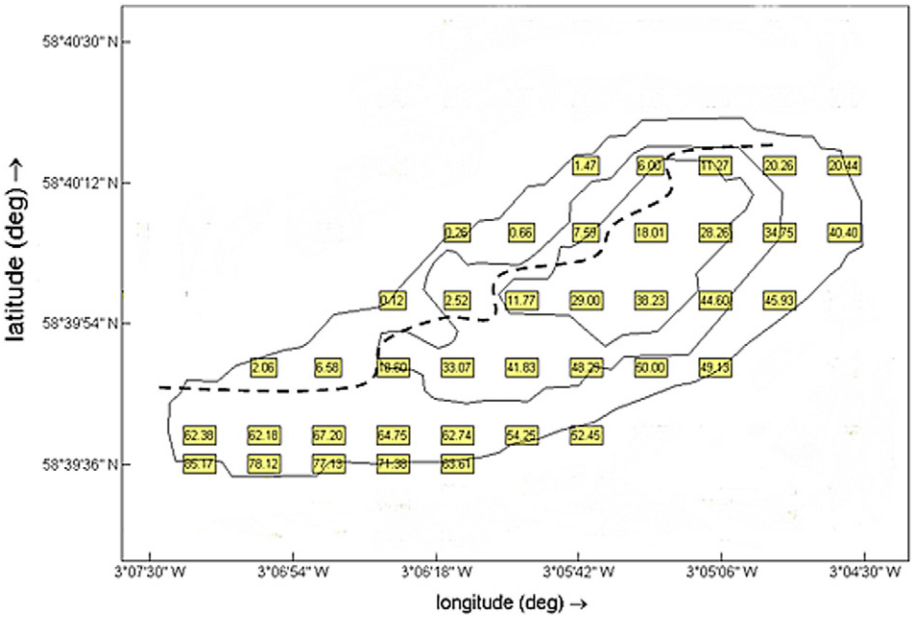

Fig. 14. Bed shear stresses (N/m^2) at maximum spring flood tide (19/09/2001 08:00) on the sandbank A. Continuous black lines denote the extent of the sandbank. The regions below the black dashed line denote the parts of maximum bed shear stresses which significantly exceed the critical bed shear stress magnitude on the southern flank of the sandbank.

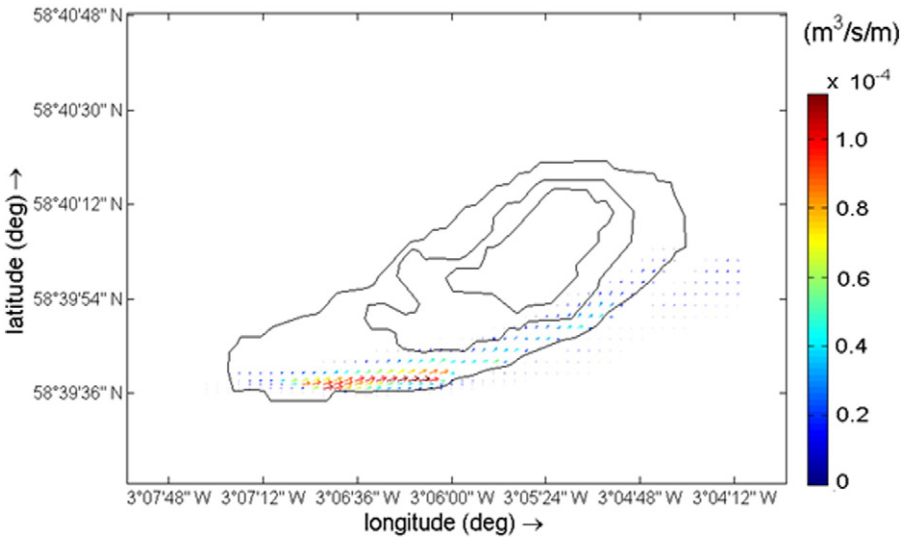

Fig. 15. Bed load sediment transport rates ($m^3/s/m$) close to slack water time (19/09/2001 11:20) on the sandbank A. Continuous black lines denote the extent of the sandbank. The colour bar indicates the magnitude of sediment transport rates and arrows indicate sediment transport direction.

ecologically important benthic communities. The morphodynamic model was run for an equivalent of two spring-neap cycles between 09/09/2001 and 09/10/2001. It is worth noting that some differences were found between the tidal current magnitudes in the first and second spring tides which may be attributed to the inclusion of the N2 constituent in model runs. Maximum currents during the first spring tide (19/09/2001) significantly increased sediment transport rates, inflicting the notable bottom level changes. In the analysis presented below the existing morphodynamic regime of the sandbanks A and B, during maximum spring tide (19/09/2001) is discussed in detail.

5.1. Sandbank A: sediment transport patterns at spring ebb phase

At spring ebb phase (19/09/2001 2:40) currents enter the east sandbank A at its northern edge, as can be seen in Fig. 7. The currents veer slightly and direct towards south-westward of the sandbank area. Bottom velocities increase gradually from the east part of the sandbank to the west. Maximum velocities are observed closer to the north-northwest flank and reach a speed of more than 2.0 m/s at the bottom layer (Fig. 7). Weak bottom currents reach velocities of less than 1.8 m/s towards the south-southeast flank.

It should be noted that over a semi-diurnal tidal cycle, currents in the bottom layer are consistently offset relative to current vectors in the surface layer. The direction of offset is the direction of the rotation of the surface current vector relative to north, at each phase of the tidal cycle. Following that it is found that the bottom ebb currents passing over the sandbank area present towards the bank crest, a maximum anticlockwise directionality offset of ~10°, in relation to surface tidal flows.

In a similar manner to ebb flows, bed load transport rates increase towards the downstream flank of the sandy wedge reaching a maximum value of $\sim 4.5 * 10^{-4}$ $m^3/s/m$. A notable reduction in transport rates is observed towards the north-northeast crest of the sandbank area ($<2 * 10^{-4}$ $m^3/s/m$) (Fig. 8). Most of the bed load transport processes occur towards the tip of the Island of Stroma, followed by a downstream increase in sediment transport rates.

Closer to the sea bed the horizontal shear stresses and tidal currents vectors have the same direction and move coarser sediment fractions as

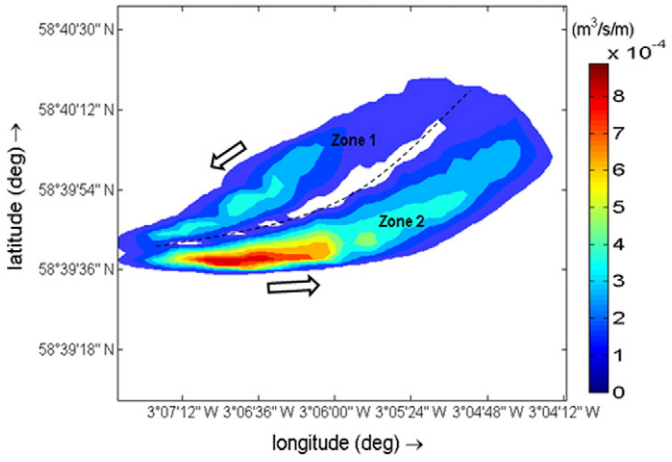

Fig. 16. Differences between maximum ebb (02:40) and flood (08:00) bed load sediment transport rates ($m^3/s/m$) covering a full spring tidal cycle (19/09/2001) on the sandbank A. The black dashed line denotes the area of sediment convergent zone. White arrows indicate the direction of ebb- (zone 1) and flood- (zone 2) dominated sediment transport. The colour bar indicates the magnitude of sediment transport rates.

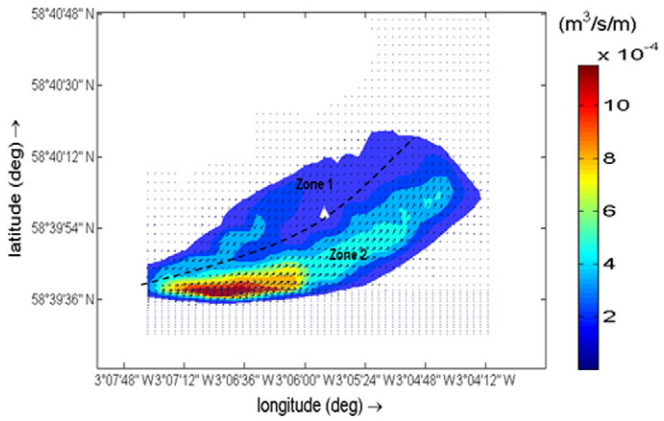

Fig. 17. Maximum bed load sediment transport rates ($m^3/s/m$) at ebb (02:40) and flood (08:00) spring tide (19/09/2001) on the sandbank A. The black dashed line denotes the area of sediment convergent zone. The colour bar indicates the magnitude of sediment transport rates and arrows indicate sediment transport direction.

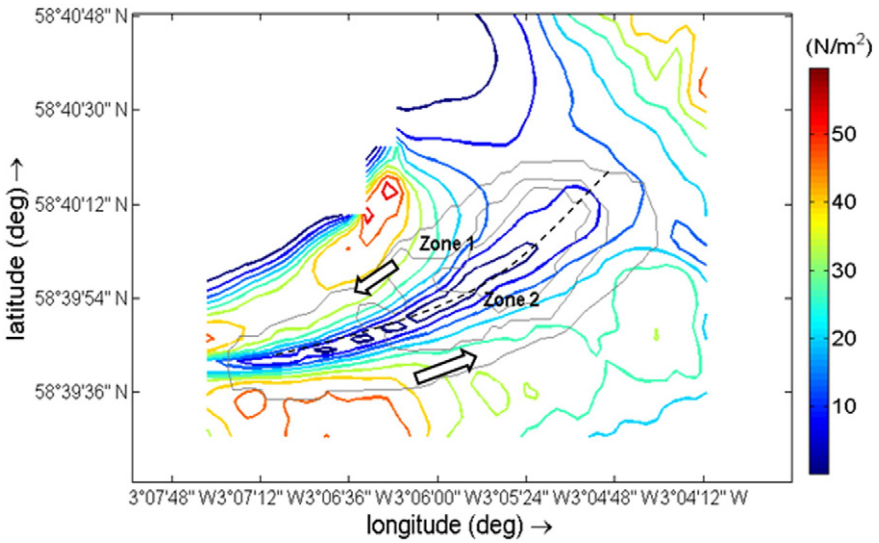

Fig. 18. Differences between maximum ebb (02:40) and flood (08:00) in bed shear stresses (N/m^2) covering a full spring tidal cycle (19/09/2001) on the sandbank A. Continuous grey lines denote the extent of the sandbank. The black dashed line denotes the area of bed shear stress convergent zone. White arrows indicate direction of ebb- (zone 1) and flood- (zone 2) dominated shear stresses. The colour bar indicates the magnitude of bed shear stresses.

bed load transport. It should be noted that bed load transport can be further affected in magnitude and direction by the bed level gradients once the sediments are in motion (Walstra et al., 2007). The modelling results show a slight change in direction of the transport gradients in relation to the bottom velocities to account for the bed slope corrections at the sandbank area.

The observed sediment transport in Figs. 7 and 8 can be explained by the bed shear stresses occurrences at spring ebb tide (19/09/2001 2:40), which are significantly larger than the critical values (Fig. 9) resulting in notable sediment transport rates over the sandbank area. For the selected $SedD_{50}$ values at the eastward crest and the westward wedge of the sandbank A (see Section 4) the critical shear stress magnitude equals to 2.21 and 1.31 N/m^2 respectively. Higher bed shear stresses can be observed closer to the north-northwest flank followed by an increase in sediment transport rates in the same direction (Fig. 8).

At neap ebb tide (26/09/2001 10:40) currents follow the same pattern as during spring ebb tide but significantly weaker flows occur on the sandbank A. Bottom velocities gradually increase in the south-westward direction and reach a maximum speed of around 0.9 m/s at the north-west flank of the sandbank. Following that, bed load transport mostly occurs in the direction of the current with peak rates reaching $0.16 * 10^{-4}$ m^3/s/m. It should be noted that most of the bed load transport at the northern flank of the sandbank area occurs during the spring ebb tide.

Closer to the end of the ebb phase of the tidal cycle (19/09/2001 05:20), bottom current velocities significantly decrease. Weaker currents flow over the sandbank and reach speeds less than 1.0 m/s at the north-west part of the sandy deposit. As a result, an overall decrease in sediment transport rates can be found where sediment movement is restricted mostly to the western edge of the northern flank (Fig. 10).

5.2. Sandbank A: sediment transport patterns at spring flood phase

At spring flood phase (19/09/2001 8:00), where surface velocities reach their maximum (up to 5.5 m/s) strong currents, which are clearly affected by the presence of the Island of Stroma, flow towards E-NE

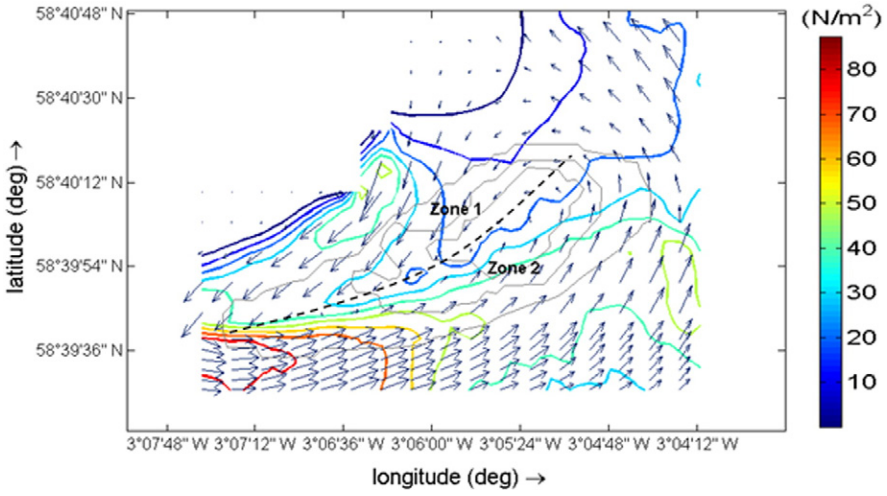

Fig. 19. Maximum bed shear stresses (N/m^2) at ebb (02:40) and flood (08:00) spring tide (19/09/2001) on the sandbank A. Continuous grey lines denote the extent of the sandbank. The black dashed line denotes the area of bed shear stress convergent zone. The colour bar indicates the magnitude of bed shear stresses and arrows indicate bed shear stress direction.

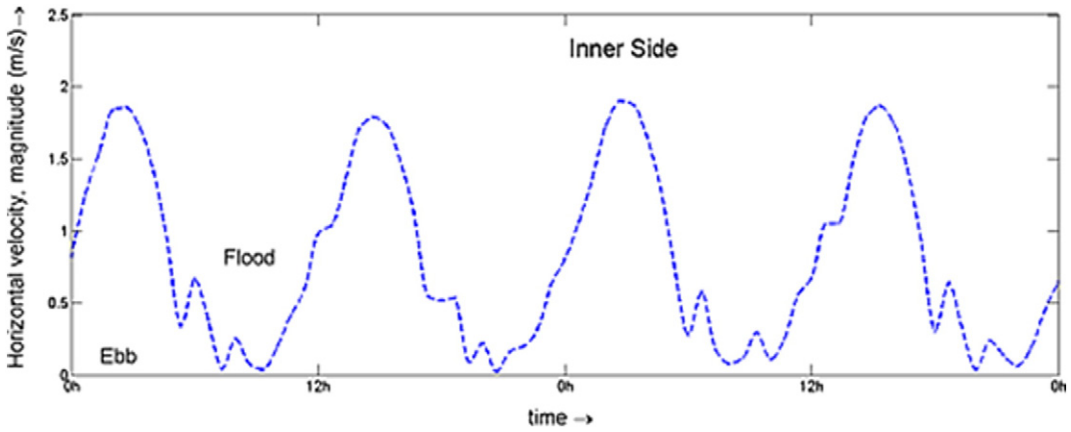

Fig. 20. Marked asymmetry in strength of the ebb and flood currents in the inner northward side of the sandbank A.

direction. As can be seen in Fig. 11, currents travel in the north-northeast direction over the sandbank A. Maximum velocities are observed closer to the south-southwest flank of the sandbank and reach a speed of more than 2.8 m/s at the bottom layer, followed by increasing velocity gradients further offshore (>3.2 m/s) (Fig. 11). Flood tidal flows significantly decrease as they cross over to the crest of the shelf bank area and towards the northern flank. Following that, weak bottom currents reach velocities of less than 0.5 m/s. In a similar manner to ebb phase, bottom currents present an anticlockwise directionality offset between 4° to 14° in relation to surface tidal flows passing over the sandbank area.

The presence of a small-scale, anticlockwise eddy can also be seen on the northern flank region. Flood currents veer and create cyclonic eddies throughout the entire water column as seen in Fig. 12, showing the horizontal velocity vectors (m/s) at surface (σ-layer 1), middle (σ-layer 5) and bottom layer (σ-layer 10) on the sandbank. It is found that those transient circulation patterns developed during that half of the tidal cycle are entirely dissipated at the next half of the cycle.

The computed bottom velocities on the sandbank area (0.5–3 m/s) show a region of very strong tidal flows. Recorded peak tidal flows are significantly larger in comparison to those seen on tidal sandbanks observed elsewhere in the vicinity of headlands/islands [e.g. velocities measured around Portland Bill, UK was less than to 1.4 m/s (Bastos et al., 2002)].

At spring flood phase, the bed load transport rates on the south-southwest flank of the bank area are significantly larger ($>10 * 10^{-4}$ m^3/s/m) than that during ebb phase, in response to strong flood currents flowing in the same direction. Peak tidal velocities reduce further downstream at the southern flank followed by a decrease in gradients in sediment transport rates. Closer to the crest and centre of the sandbank sediment transport rates are significantly low ($<2 * 10^{-4}$ m^3/s/m). Tidal flows decrease in magnitude as they travel and exit the sandbank area at its northern side followed by a notable decrease in sediment transport rates (Fig. 13).

At neap flood tide (26/09/2001 16:40) currents follow the same pattern and significantly weaker flows are present towards the southern flank of the sandbank area. Maximum bottom velocities reach 1.4 m/s at the south-west edge of the bank with sediment transport rates approaching $0.6 * 10^{-4}$ m^3/s/m. In the similar manner to ebb phase, sediment transport at spring flood tide is significantly larger than that during neap flood tide. It is found that the exceedance probability of the critical shear stress magnitude during a spring tidal cycle (19/09/2001) is 30% higher than during the neap tidal cycle (26/09/2001). Following these observations, it can be stressed that sediment transport leading to notable morphological changes at the bank region occurs mostly during the spring tide.

It is noted that sediment transport patterns do not necessarily follow the flow pattern. Bed load transport is a non-linear process (Roos et al., 2001; Bastos et al., 2003). The existence of a shelf bank area where generally strong currents occur may depend on the dynamic balance of sediment dynamics, which are mainly driven by the spatially and temporarily varying currents and the excess bed shear stresses around the bank (Soulsby, 1981). The above process in action is quite apparent at the north flank of the sandbank region, where sediment transport does not follow the observed, anticlockwise transient eddy of the tidal current (Fig. 12). Here, the weak tidal currents in circulation do not

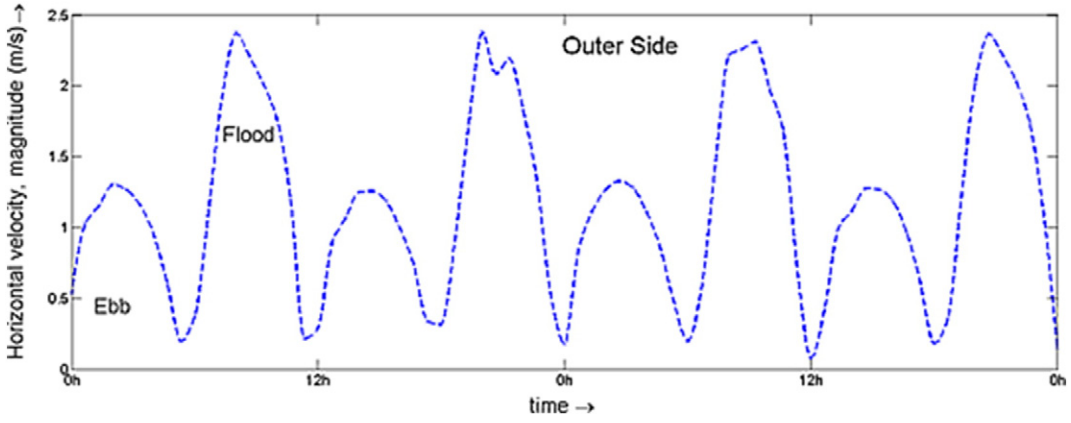

Fig. 21. Marked asymmetry in strength of the ebb and flood currents in the outer southward side of the sandbank A.

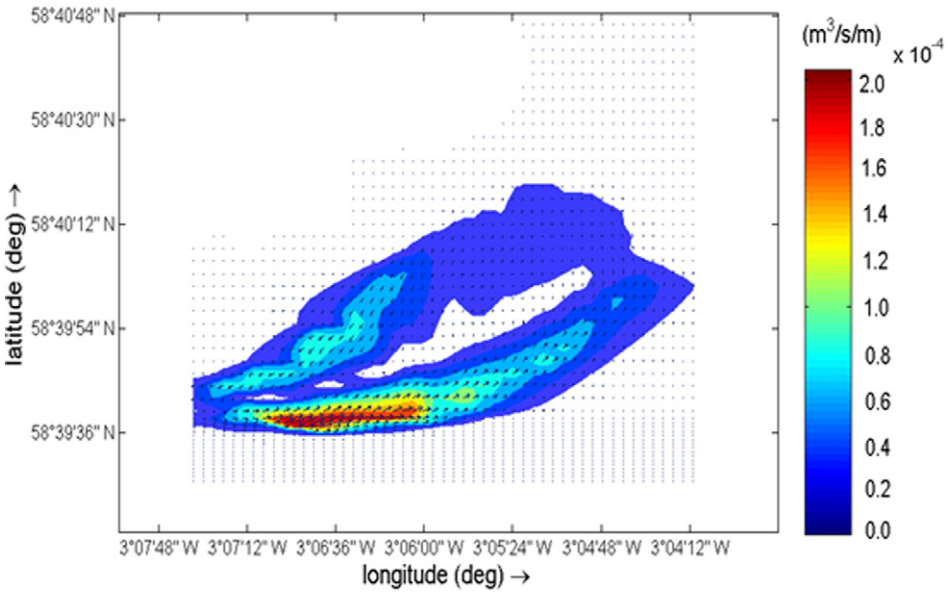

Fig. 22. Residual bedload sediment transport rates ($m^3/s/m$) for a spring tidal cycle (19/09/2001) on the sandbank A. The colour bar indicates the magnitude of sediment transport rates and arrows indicate sediment transport direction.

allow bed shear stresses that exceed the critical bed shear stress to move the sediment. However, the opposite is true on the southern flank of sandbank A, as can be seen in Fig. 14.

It is found that throughout the development of those transient circulation patterns sediment transport rates significantly increase in a constrained zone between the crest/centre and the southern flank of the sandbank area (Fig. 13). In contrast, significant sediment transport rates can be observed over the whole bank area at spring ebb phase (19/09/2001 2:40) (Fig. 8). The reductions in transport rates towards the centre/crest of the sandbank area during both the peak flood and ebb phase indicate a distinct sand accretion area.

Bottom current velocities are significantly smaller (<1.8 m/s) close to slack water time (19/09/2001 11:20), resulting in an overall decrease in sediment transport rates. Sediment movement is confined to the western most part of the southern flank where bed load transport rates are less than $<1 * 10^{-4}$ $m^3/s/m$ (Fig. 15). In a short period of time after slack water (04/10/2001 12:00), bottom currents are further decreased (<0.8 m/s). Flow gradually reverses and weak ebb currents enter the bank area from its northern side. Currents flow southwards and insignificant sediment transport rates can be observed along the northwest side of the sandbank, which reach a maximum value of $0.2 * 10^{-4}$ $m^3/s/m$.

5.3. Sandbank A: net sediment transport patterns and bed form dynamics

Modelling the existing morphodynamic regime of the sandbank A during two spring-neap tidal cycles reveals that the shelf bank area is dynamic under the existing flow regime. Computed results of the differences in maximum sediment transport during the ebb and flood phases of a spring tidal cycle (19/09/2001) reveal an anticlockwise sediment circulation pattern over the sandbank A. Following that, an eastward net flood dominated sediment transport is observed as shown in Fig. 16. In Fig. 16, two distinct zones of bed load transport have been recognized. At the northern flank of the sandbank a net sediment transport pathway (zone 1) can be observed with increasing sediment transport gradients towards the tip of the island. Across

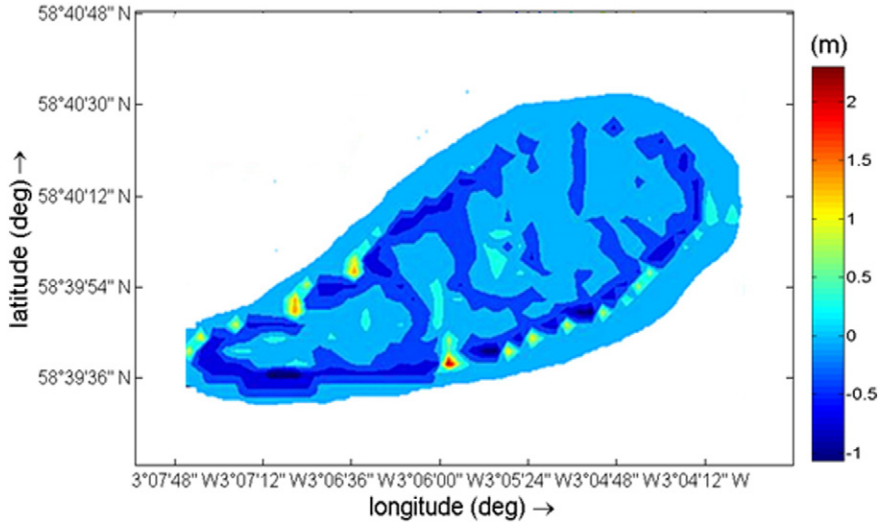

Fig. 23. Cumulative erosion/accretion (m) on the sandbank A over one month's period (from 09/09/2001 to 09/10/2001). The colour bar indicates the magnitude of cumulative erosion (negative values) and cumulative accretion (positive values).

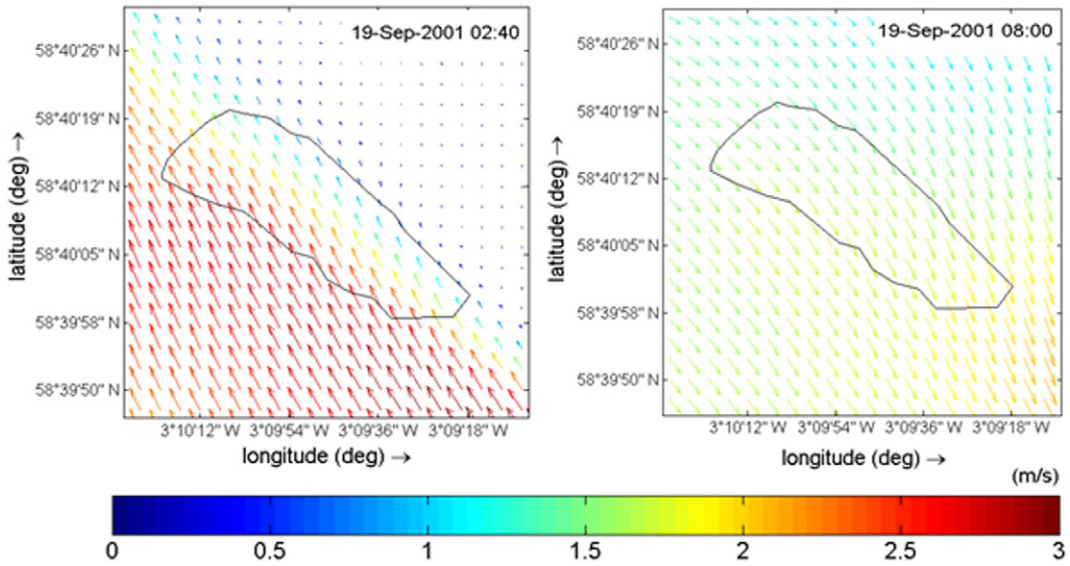

Fig. 24. Horizontal velocity at the bottom layer (m/s) at maximum spring (19/09/2001) ebb (02:40) (left) and flood tide (8:00) (right) on the sandbank B. Continuous black lines denote the extent of the sandbank. The colour bar indicates the magnitude of velocity and arrows indicate velocity direction.

the southern part of the shelf bank area (zone 2) even higher sediment transport rates are observed further offshore from the tip of the Island of Stroma which gradually decrease downstream in the south-eastward direction. The two discrete sediment transport areas result in a convergent zone where sediments rest towards the centre of the sandbank.

It was found that sediment transport is larger during peak ebb (19/09/2001 02:40) and flood (19/09/2001 08:00) flows than during the rest of the tidal cycle, where bed load transport rates reach a maximum value of ~$10 * 10^{-4}$ $m^3/s/m$ at the south-western part of the bank area at spring flood phase (Fig. 17).

The difference in bed shear stresses during maximum ebb (02:40) and flood (08:00) of the spring tidal cycle (19/09/2001) reveal an intermediate boundary, formed by decreasing shear stress gradients between two zones (Baston and Harris, 2011; Baston et al., 2013) at the sandbank area (Fig. 18). It is found that the internal boundary coincides with the observed sediment transport convergent zone shown in Fig. 16. Bed shear stresses significantly increase towards the tip of the Island of Stroma and closer to Mell Head and reach values higher than 80 N/m^2. Shear velocities lie within the range 0.04–0.20 m/s and maximum bed shear stress magnitude varies from 18 to 75 N/m^2 (Fig. 19).

Peak tidal flows indicate the predominant direction of sediment transport (Johnson et al., 1982). Eulerian monitoring points located at the northern flank in the inner side of the shelf bank area during a spring tidal cycle (19/09/2001) reveal stronger ebb currents compared to flood currents where flood flows reach a maximum speed of less than 0.5 m/s (Fig. 20). As a result, sediments tend to move in the ebb direction. In contrast, at the outer side southwards, stronger flood flows move sediments in the direction of the peak flood currents (Fig. 21).

It should be noted that the residual bed load transport shows the resultant net sediment transport patterns during a tidal cycle. The residual sediment transport at the sandbank area over the tidal cycle was computed using simulated flows during a full spring tidal cycle (19/09/2001) taking the mean value of the bed load transport rates at each time step and at each node of the morphodynamic grid, following Bastos et al. (2003) (Fig. 22).

It was found that the residual bed load transport on the sandbank A is significantly low where the maximum value, which occurs at the south-western part of the sandbank, is about $2 * 10^{-4}$ $m^3/s/m$. Observed net ebb-dominated transport rates closer to the tip of the Island of Stroma and flood-dominated transport rates away from the island form a distinct anticlockwise sediment transport circulation pattern at

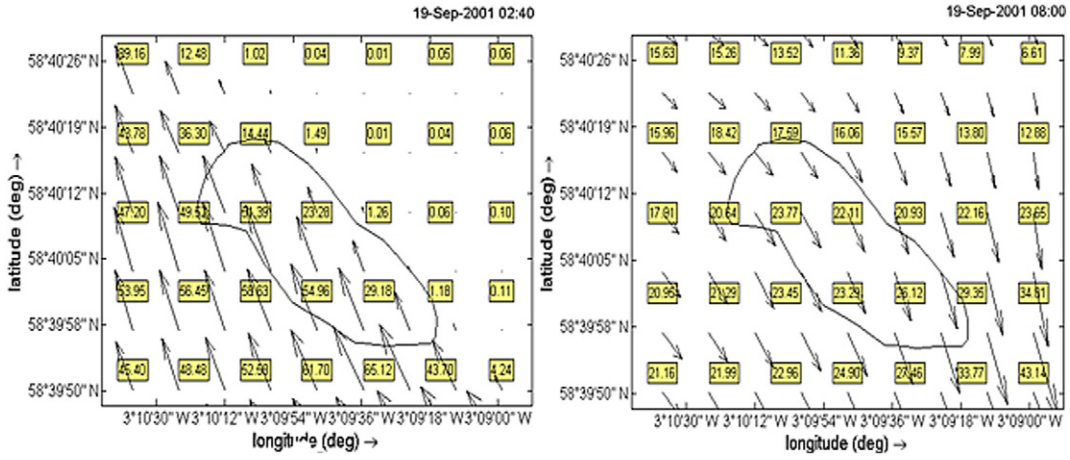

Fig. 25. Bed shear stresses (N/m^2) at maximum spring (19/09/2001) ebb (02:40) (left) and flood (08:00) (right) tide on the sandbank B. Continuous black lines denote the extent of the sandbank. Arrows indicate bed shear stress direction.

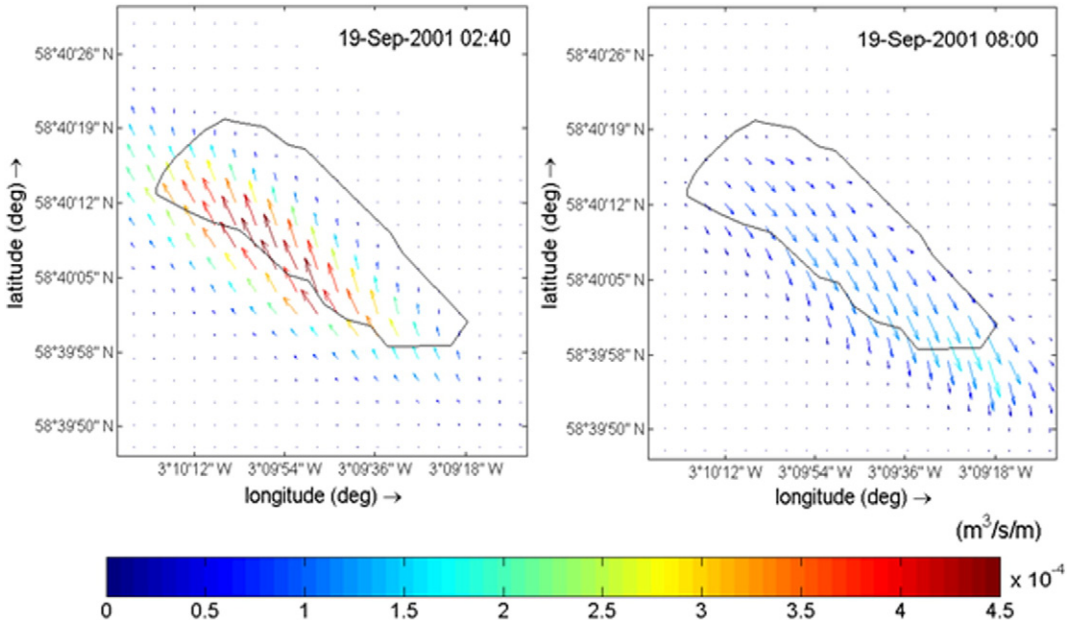

Fig. 26. Bed load sediment transport rates ($m^3/s/m$) at maximum spring (19/09/2001) ebb (02:40) (left) and flood (08:00) (right) tide on the sandbank B. Continuous black lines denote the extent of the sandbank. The colour bar indicates the magnitude of sediment transport rates and arrows indicate sediment transport direction.

the shelf bank area. The resultant cumulative erosion/accretion at the sandbank may be driven by the observed residual sediment transport rates over a tidal cycle. As can be seen in Figs. 22 and 23, decreasing bed load transport rates in the transport direction lead to accretion whereas increasing transport will result in small regions of erosion on the sandbank area during the two spring-neap cycles considered in this study.

Positive/negative sediment transport gradients can lead to erosion or deposition. High sediment transport rates alone may at times often result in less significant morphological changes however, when the transport gradients are larger, large bed changes can be seen (Roelvink and Reniers, 2012). On the sandbank A, gradual changes to transport gradients along with low sediment transport rates resulted in small morphological changes over one month period (Fig. 23).

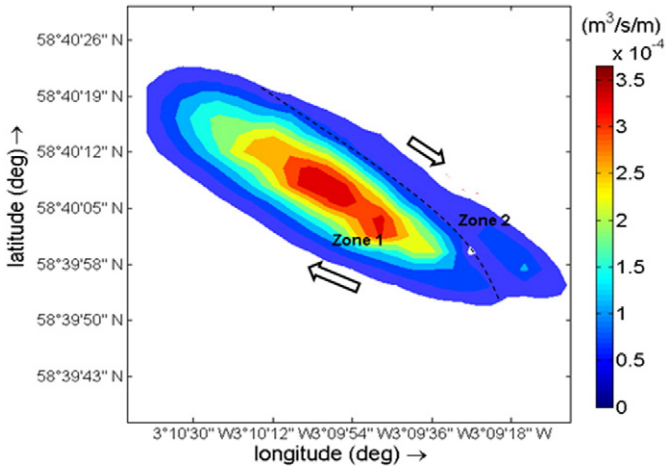

Fig. 27. Differences between maximum ebb (02:40) and flood (08:00) bed load sediment transport rates ($m^3/s/m$) covering a full spring tidal cycle (19/09/2001) on the sandbank B. The black dashed line denotes the area of sediment convergent zone. White arrows indicate the direction of ebb- (zone 1) and flood- (zone 2) dominated sediment transport. The colour bar indicates the magnitude of sediment transport rates.

However it is important to note that changes are likely to be greater over long-term morphodynamic scales (annual to decadal scale). Minor changes of centimetres over one month can be equivalent to several metres when scaled up to years.

6. Morphodynamics of the sandbank B

6.1. Sandbank B: sediment transport patterns over one spring tidal cycle

At spring ebb phase (19/09/2001 2:40) near-bed currents flow north-westward at the sandbank B. A gradient in bottom velocities is observed from the south-west flank of the sandbank to the north-east side. Tidal flows at the seabed at the eastern part of the bank are significantly weaker than that at the western part and reach a maximum of 1.5 m/s (Fig. 24). At spring flood phase (19/09/2001 8:00) maximum velocities can be observed closer to the south-southeast flank and reach a maximum of 2 m/s, followed by decreasing velocities towards the north-westward (<1.6 m/s) (Fig. 24).

It should be noted that the computed bottom velocities over the sandbank B (0.9–2.8 m/s) show a region of strong tidal flows. As can be seen in Fig. 25, bed shear stresses on the sandbank B significantly exceed the critical shear stress required to move the sediments, which for the selected $SedD_{50}$ value (see Section 4) is equal to 3.21 N/m^2. Sediment transport rates reach a maximum value of $4.65 * 10^{-4}$ $m^3/s/m$ on the south-west flank of the sandbank (Fig. 26). A decreasing gradient in bed load transport is further observed to the eastwards, away from the tip of the Island of Stroma. At spring flood phase, sediment transport gradient decreases towards the south-eastward part of the bank. Bed load transport direction exhibits a slight clockwise veering, in response to strong flood currents and transport rates reach a maximum low value of $1.6 * 10^{-4}$ $m^3/s/m$ towards the tip of Stroma (Fig. 26).

Maximum bed shear velocities are not evenly distributed around the tip of the Island of Stroma during a spring tidal cycle (19/09/2001). It seems that the localized interactions between currents and sea bed topography highly influence and asymmetrically distribute bed velocities on the bank areas during the tidal cycle. The currents at both spring ebb and flood tide accelerate closer to the tip of Island of Stroma and decrease in magnitude further offshore. The intensity of the accelerated current depends on the width to length (w/l) ratio of the island and

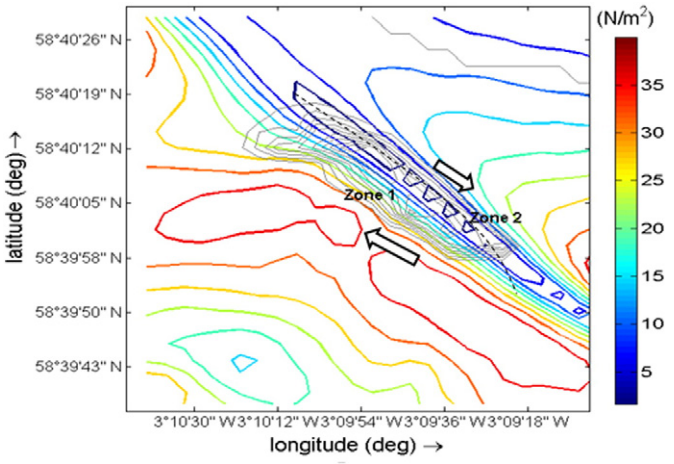

Fig. 28. Differences between maximum ebb (02:40) and flood (08:00) in bed shear stresses (N/m2) covering a full spring tidal cycle (19/09/2001) on the sandbank B. Continuous black lines denote the extent of the sandbank. The black dashed line denotes the area of bed shear stress convergent zone. White arrows indicate direction of ebb- (zone 1) and flood- (zone 2) dominated shear stresses. The colour bar indicates the magnitude of bed shear stresses.

the asymmetric geometry of the island's tip (White and Wolanski, 2008). The numerical case study of White and Wolanski (2008) states that for w/l ratios greater than 0.25, as is the case of Stroma where the ratio equals to ~0.45 and for less sharp-edged tips, accelerating currents are more intense. The southern tip of Stroma (see Fig. 4) presents an asymmetry. Flood flows approaching from its west side face a less-sharp edged tip, in comparison to ebb flows flowing from the east side. As a result, during spring ebb tide, velocities which increase in the westward direction reach a maximum value of 0.2 m/s closer to the tip of the island. However, a shift of more intense velocities to the eastward is observed during spring flood tide, which reaches 0.23 m/s in the lee of the island. The intensity of the velocity field on both sandbanks highly depends on the locality with respect to island's tip. The velocities are higher on the eastward sandbank A (0.02–0.20 m/s) lying closer to Stroma than on the westward sandbank B (0.03–0.18 m/s) which is located further from the Island of Stroma. It should be noted that overall, the maximum bed velocity occurred here is significantly larger than that reported elsewhere in the vicinity of headlands/islands, (e.g. that observed around Portland Bill, UK was around 0.1 m/s, Bastos et al. (2002)).

At neap tide (26/09/2001) weaker currents follow the same pattern. Maximum near-bed ebb (10:40) currents reach 1 m/s to the westward flank of the bank followed by peak sediment transport rates of $0.02 * 10^{-4}$ $m^3/s/m$. It should be noted that sediment transport processes mostly occur at spring tide.

6.2. Sandbank B: net sediment transport patterns and bed form dynamics

The existing morphodynamics of the sandbank B were modelled over a period of two spring-neap tidal cycles. Results on the differences in maximum sediment transport rates covering a spring tide (19/09/2001) reveal a clockwise circulation pattern on the small bank (Fig. 27). A north-eastward ebb dominated sediment transport can be observed and two zones of sand movements in opposite direction have been recognized. Higher sediment transport rates are found in the western flank (zone 1). Transport gradients decrease northwards, forming a convergent zone where sediments are deposited. As a result, the sandbank B has taken a more elongated shape. Across the eastern part of the sandbank (zone 2) small sediment transport rates are observed towards south-eastward direction.

As already noted, the differences in maximum bed shear stresses during ebb (02:40) and flood (08:00) spring cycle (19/09/2001) change sediment transport rates during flood and ebb tide (Fig. 28). As a result, an internal boundary is formed where decreased gradients in bed shear stresses coincide with the sediment transport convergent zone denoted in Fig. 27.

The resultant cumulative erosion and accretion patterns of the sandbank can be determined by the observed residual (mean) sediment transport rates, which have been computed for a period covering a spring tide (19/09/2001) (Fig. 29). Observed net ebb-dominated transport rates away from and flood–dominated transport towards the Island of Stroma form a distinct clockwise sediment transport circulation pattern. The sandy deposits on the bank erode southwards; in response

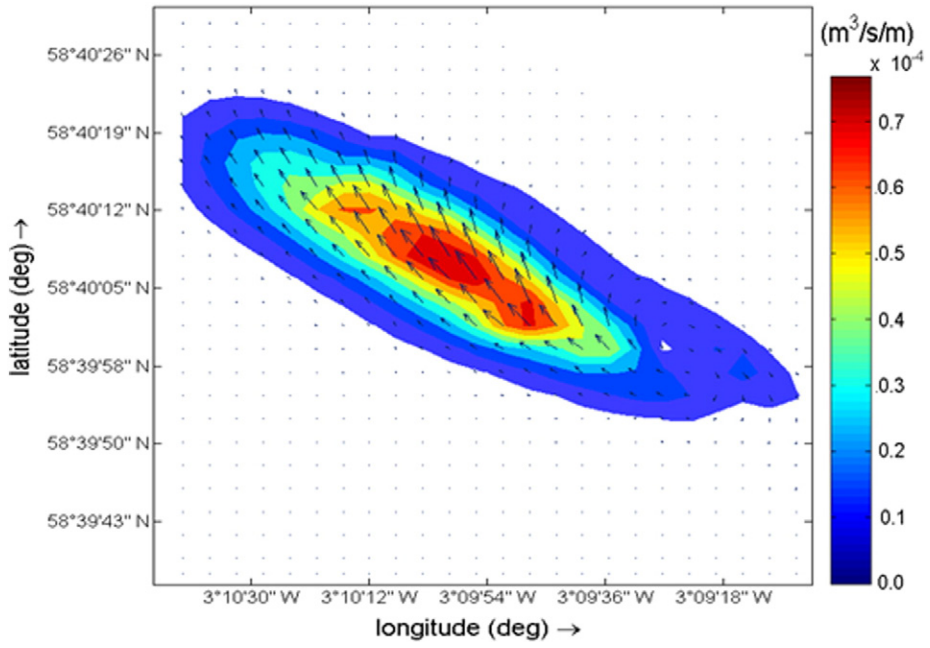

Fig. 29. Residual bedload sediment transport rates ($m^3/s/m$) for a spring tidal cycle (19/09/2001) on the sandbank B. The colour bar indicates the magnitude of sediment transport rates and arrows indicate sediment transport direction.

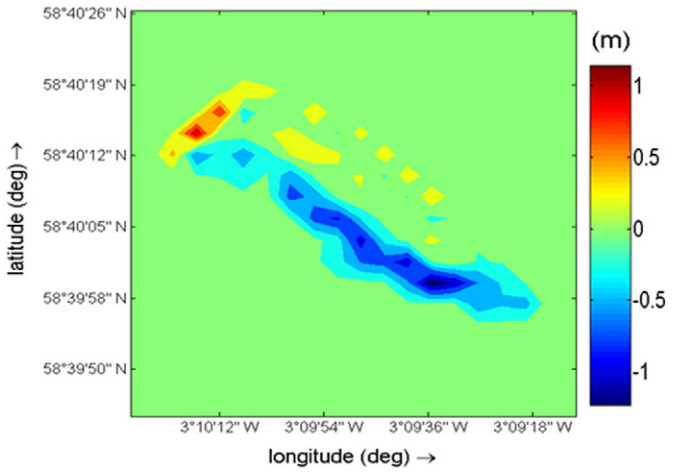

Fig. 30. Cumulative erosion/accretion (m) on the sandbank B area over one month's period (from 09/09/2001 to 09/10/2001). The colour bar indicates the magnitude of cumulative erosion (negative values) and cumulative accretion (positive values).

to increasing transport rates towards the sandbank centre/crest whereas sediments mostly move and accumulate at the northern part of the shelf bank area.

As can be seen in Fig. 30, a notable bed change can be observed on the sandbank B during two spring-neap tidal cycles. Sediments travel northward and reshape the bank into a more elongated shape. The sandbank volume is preserved but the bank feature seems quite mobile. Ebb-dominated, residual transport rates consistently rework sediments since they are mostly driven by the asymmetry found between the ebb and the flood currents inside the channel. However, due to the unavailability of measured data on sandbank dynamics, further investigation of this is not possible.

7. Concluding remarks

In this study a high resolution 3D hydrodynamic-morphodynamic model was used to explore the morphodynamics of two substantial sandbanks A, B located in the Inner Sound channel of Pentland Firth, Scotland, UK. The sandbanks lie on offshore seabed where water depth exceeds 18 m. Sediment availability in Pentland Firth is limited however sandy deposits lie on the scoured bed rock in some regions. We described sand coverage inside the Pentland Firth, Inner Sound channel via interrogation of data provided by the MSS (2010) video trawls, BGS (2013) particle size data and the geological conditions available in the MeyGen EIA Quality Mark Report (MeyGen, 2012).

Hydrodynamic simulations from a fully validated regional Pentland Firth model provided the boundary conditions for the high resolution 3D local scale hydrodynamic-morphodynamic model of the Inner Sound. Investigation of the sandbanks dynamics for a period of two spring-neap tidal cycles showed that they are dynamic and variable under the existing flow regime. Bed shear stresses on the sandbank areas significantly exceeded the critical values required for sediment movement only during maximum ebb and flood flows. The sediment eventually moved over time in the direction of relatively low residual sediment transport rates. Positive/negative residual sediment transport gradients led to erosion or accretion patterns on the two sandbanks.

Bed shear velocity magnitudes, which in turn controlled sediment transport, were higher on the sandbank A than on the sandbank B. It was found that the interactions between highly energetic currents and local sea bed topography influence and unevenly distribute bed shear velocities on the two sandbank areas.

On sandbank A, an eastward flood-dominated sediment transport was observed. The sandbank eroded on the flank regions and sediment settled towards the central parts of the bank. Small bed level changes occurred over one month period, which are likely to be higher over long term morphodynamic scales (years to decades) if same trends continue over long periods of time, which may have potential effect on the local macrobenthos and species diversity. On sandbank B, a northward ebb-dominated sediment transport induced notable sandbank movement. The sandbank volume was preserved but the sandy feature was quite mobile. Ebb-dominated, residual transport rates consistently moved sediments northward and reshaped the west bank in a more elongate shape.

As a result of the prevalence of extremely large tidal currents, the Inner Sound Channel of Pentland Firth is a highly favoured area for in-stream tidal power developments. The results indicate that the complex flow structure present in the Inner sound channel is responsible for the formation, maintenance and evolution of the sandbanks investigated in this study. The results also reveal that as the location and the morphology of the sandbanks are strongly linked with the existing hydrodynamic regime, any changes to flow field as a result of tidal stream energy extraction may significantly alter the dynamics of the banks, thus leading to erosion/accretion or migration. Therefore, this modelling study gives useful insight to potential impacts of tidal stream energy generation installations on these delicate sea bed features. Further study using the current modelling setup is in progress to map those impacts.

Acknowledgements

AC wishes to acknowledge College of Engineering of Swansea University and EA/Welsh Government funded Low Carbon Research Institute (LCRI) for the studentship provided to pursue her PhD research. HK acknowledges EPSRC funded Terawatt project (EP/J010170/1) and Ecowatt project (EP/K012851/1) for providing data used in this study.

References

Baston, S., Harris, R.E., 2011. Modelling the hydrodynamic characteristics of tidal flow in the Pentland Firth. Proceedings of the 9th European Wave and Tidal Energy Conference, Southampton, UK, 5–9 September 2011.

Baston, S., Harris, R., Woolf, R., Hiley, R.A., Side, J.C., 2013. Sensitivity analysis of the turbulence closure models in the assessment of tidal energy resource in Orkney. Proceedings of the 11th European Wave and Tidal Energy Conference, Aalborg, Denmark, 2–5 September 2013.

Bastos, A.C., Collins, M.B., Kenyon, N.H., 2003. Water and sediment movement around a coastal headland: Portland Bill, Southern UK. Ocean Dyn. 53 (3), 309–321. http://dx.doi.org/10.1007/s10236-003-00311.

Bastos, A.C., Kenyon, N.H., Collins, M., 2002. Sedimentary processes, bedforms and facies, associated with a coastal headland: Portland Bill, Southern UK. Mar. Geol. 187 (3–4), 235–258.

Bastos, A.C., Paphitis, D., Collins, M.B., 2004. Short-term dynamics and maintenance processes of a headland-associated sandbank: shambles bank, English Channel (UK). Estuar. Coast. Shelf Sci. 59 (1), 33–47. http://dx.doi.org/10.1016/j.ecss.2003.07.008.

Berthot, A., Pattiaratchi, C., 2006. Mechanisms for the formation of headland-associated linear sandbanks. Cont. Shelf Res. 26 (8), 987–1004. http://dx.doi.org/10.1016/j.csr.2006.03.004.

British Geological Survey, 2013. BGS Legacy Particle Size Analysis Uncontrolled Data Export. Supplier: EPSRC Funded Terawatt Project EP/J010170/1.

Chatzirodou, A., Karunarathna, H., 2014. Impacts of tidal energy extraction on sea bed morphology. Coast. Eng. Proc. 1 (34). http://dx.doi.org/10.9753/icce.v34.sediment.33 (sediment.33).

Couch, S.J., Bryden, I.G., 2008. Tidal current energy extraction: hydrodynamic resource characteristics. Proc. Inst. Mech. Eng. M J. Eng. Marit. Environ. 220, 185. http://dx.doi.org/10.1243/14750902JEME50.

Deltares, 2011. Delft3D-QUICKIN Generation and manipulation of grid-related parameters such as bathymetry, initial conditions and roughness User Manual Version: 4.00. Delft: Deltares.

Dyer, K.R., Huntley, D.A., 1999. The origin, classification and modelling of sand banks and ridges. Cont. Shelf Res. 19, 1285–1330. http://dx.doi.org/10.1016/S0278-4343(99)00028.

Easton, M., Woolf, D.K., Harendza, A., Jackson, A., 2011. Characterization of a tidal energy site: hydrodynamics and seabed structure. Proceedings of the 9th European Wave and Tidal Energy Conference, Southampton, UK, 5–9 September 2011.

Easton, M.C., Woolf, D.K., Pans, S., 2010. An operational hydrodynamic model of a key tidal-energy site: inner sound of Stroma, Pentland Firth (Scotland, UK). Proceedings of the 3rd International Conference on Ocean Energy, Bilbao, Spain, 06–08 October 2010.

Egbert, G.D., Bennett, A.F., Foreman, M.G.G., 1994. TOPEX/POSEIDON tides estimated using a global inverse model. J. Geophys. Res. Oceans 99, 24821–24852. http://dx.doi.org/10.1029/94JC01894 (1978-2012).

EOEA (European Ocean Energy Association), 2012. European ocean energy roadmap 2010–2050. Retrieved May 6, 2014, from: http://www.erec.org/fileadmin/erec_docs/Documents/Publications/European%20Ocean%20Energy%20Roadmap_2010.pdf.

Fallon, D., Hartnett, M., Olbert, A., Nash, S., 2014. The effects of array configuration on the hydro-environmental impacts of tidal turbines. Renew. Energy 64, 10–25. http://dx.doi.org/10.1016/j.renene.2013.10.035.

Goddijn-Murphy, L.M., Woolf, D.K., Easton, M., 2013. Current patterns in the Inner Sound (Pentland Firth) from underway ADCP data. J. Atmos. Ocean. Technol. 30 (1), 96–111. http://dx.doi.org/10.1175/JTECH-D-11-00223.1.

iXSurvey, 2009. Geophysical site survey to provide an indication of the seabed substratum present in the Inner Sound (PF, UK). Retrieved April 14, 2014, from: http://www.ixsurvey.com/en/index.php/projects/scottish-power-renewables-tidal-turbine-site-surveys/.

Johnson, M.A., Kenyon, N.H., Belderson, R.H., Stride, A.H., 1982. Sand Transport. In: Stride, A.H. (Ed.), Offshore Tidal Sands: Processes and Deposits. Chapman and Hall, London, pp. 58–94.

Jones, O.P., Simons, R.R., Jones, E.J.W., Harris, J.M., 2006. Influence of seabed slope and Coriolis effects on the development of sandbanks near headlands. J. Geophys. Res. 111 (C3). http://dx.doi.org/10.1029/2005JC002944.

Kleinhans, M.G., Van Rijn, L.C., 2002. Stochastic prediction of sediment transport in sand-gravel bed rivers. J. Hydraul. Eng. 128 (SPECIAL ISSUE: STOCHASTIC HYDRAULICS AND SEDIMENT TRANSPORT), 412–425. http://dx.doi.org/10.1061/(ASCE)0733-9429(2002)128:4(412).

Lefebvre, A., Paarlberg, A.J., Winter, C., 2014. Flow separation and shear stress over angle-of repose bed forms: a numerical investigation. Water Resour. Res. 50 (2), 986–1005. http://dx.doi.org/10.1002/2013WR014587.

Lesser, G.R., Roelvink, J.A., Van Kester, J.A.T.M., Stelling, G.S., 2004. Development and validation of a three-dimensional morphological model. Coast. Eng. 51 (8–9), 883–915. http://dx.doi.org/10.1016/j.coastaleng.2004.07.014.

Marine Scotland Science (MSS), 2010. Database of Benthic Video Trawls. Supplier: EPSRC Funded Terawatt Project EP/J010170/1.

MeyGen, 2012. MeyGen coastal processes modelling: modelling setups, calibration and results incl. addendum. A Final Report. (Report No. SG5390 MeyGen Coastal Processes). DHI Water & Environment (S) Pte. Ltd, Singapore.

Neill, S.P., Jordan, J.R., Couch, S.J., 2012. Impact of tidal energy converter (TEC) arrays on the dynamics of headland sandbanks. Renew. Energy 37 (1), 387–397. http://dx.doi.org/10.1016/j.renene.2011.07.003.

Neill, S.P., Litt, E.J., Couch, S.J., Davies, A.G., 2009. The impact of tidal stream turbines on large scale sediment dynamics. Renew. Energy 34, 2803–2812. http://dx.doi.org/10.1016/j.renene.2009.06.015.

Nelson, J., Shreve, R.L., McLean, S.R., Drake, T.G., 1995. Role of near-bed turbulence structure in bed load transport and bed form mechanics. Water Resour. Res. 31 (8), 2071–2086. http://dx.doi.org/10.1029/95WR00976.

Robins, P.E., Neill, S.P., Lewis, M.J., 2014. Impact of tidal-stream arrays in relation to the natural variability of sedimentary processes. Renew. Energy 72, 311–321. http://dx.doi.org/10.1016/j.renene.2014.07.037.

Roelvink, D., Reniers, A., 2012. A Guide to Modelling Coastal Morphology. Advances in Coastal and Ocean Engineering. Mainland Press Pte Ltd, Singapore.

Roos, P.C., Hulscher, S.J.M.H., Peters, B.G.T.M., Nemeth, A.A., 2001. A simple morphodynamic model for sand banks and large-scale sand pits subject to asymetrical tides. Second IAHR Symposium on River, Coastal and Estuarine Mophodynamics, RCEM, Ibihiro, Japan, September 10–14, 2001.

Schlezinger, D.R., Taylor, C.D., Howes, B.L., 2013. Assessment of zooplankton injury and mortality associated with underwater turbines for tidal energy production. Mar. Technol. Soc. J. 47, 142–150. http://dx.doi.org/10.4031/MTSJ.47.4.5.

Shields, M.A., Dillon, L.J., Woolf, D.K., Ford, A.T., 2009. Strategic priorities for assessing ecological impacts of marine renewable energy devices in the Pentland Firth (Scotland, UK). Mar. Policy 33, 635–642. http://dx.doi.org/10.1016/j.marpol.2008.12.013.

Soulsby, R.L., 1981. Measurements of the Reynolds stress components close to a marine sand bank. Mar. Geol. 42, 35–47.

Soulsby, R.L., 1997. Dynamics of Marine Sands: A Manual for Practical Applications. Telford, London.

van Rijn, L.C., 1993. Principles of Sediment Transport in Rivers, Estuaries and Coastal Seas. Aqua Publications, The Netherlands.

van Rijn, L.C., 2005. Unified view of sediment transport by currents and waves. I: initiation of motion, bed roughness, and bed-load transport. J. Hydraul. Eng. 133 (6), 649–667. http://dx.doi.org/10.1061/(ASCE)0733-9429(2007)133:6(649).

Waggitt, J.J., Scott, B.E., 2014. Using a spatial overlap approach to estimate the risk of collisions between deep diving seabirds and tidal stream turbines: a review of potential methods and approaches. Mar. Policy 44, 90–97. http://dx.doi.org/10.1016/j.marpol.2013.07.007.

Walstra, D., van Rijn, L., van Ormondt, M., Brière, C., Talmon, A., 2007. The effects of bed slope and wave skewness on sediment transport and morphology. Coast. Sed. 07, 137–150. http://dx.doi.org/10.1061/40926(239)11.

White, L., Wolanski, E., 2008. Flow separation and vertical motions in a tidal flow interacting with a shallow-water island. Estuar. Coast. Shelf Sci. 77, 457–466. http://dx.doi.org/10.1016/j.ecss.2007.10.003.